Review: monoclinic zirconia, its surface sites and their interaction with carbon monoxide

Sonja Kouva,*[a] Karoliina Honkala,[b] Leon Lefferts[ac] and Jaana Kanervo[a]

This review concerns monoclinic zirconia, its surface sites and their probing with carbon monoxide. The modifications of the surface sites using thermal treatments with vacuum or reactive gases are also included. In this work, we present information on the nature and manipulation of hydroxyl species and their quantities on the surface, the different types of cationic sites where CO is adsorbed linearly and their energetics, as well as the surface sites and dynamics of formate formation. We also compare the surface concentrations of the different surface species to better understand the extent and nature of the interactions. Finally, we discuss some of the remaining open questions and how to approach them.

1. Introduction

Zirconium oxide has gained interest as both a catalyst support and a catalyst on its own, mostly due to its weak acid and basic sites[1] and stability under oxidizing and reducing atmospheres.[2] It has been an interesting catalyst material especially for biomass-related reactions that are actively investigated, as the future is bright for non-fossil fuels and chemicals. Biomass-related reaction networks usually include carbon oxides, as both carbon and oxygen are largely abundant in the starting material.

Monoclinic zirconia (also known as baddeleyite) is an oxide typically covered with hydroxyl species, similar to many metal oxides[3] used as catalysts and catalyst support materials. The structure of monoclinic zirconia provides a more versatile surface than that of other polymorphs (cubic, tetragonal) due to a less symmetrical lattice.[4] The surface sites of monoclinic zirconia include hydroxyls,[5] oxygen vacancies,[6] coordinatively unsaturated (c.u.s.) Zr–O pairs,[7] and Lewis acid sites (Zr^{3+}, Zr^{4+}).[8] The hydroxyl groups on the surface can be manipulated by thermal treatment in vacuum or in different atmospheres,[9] which are often necessary for catalytic applications, *e.g.*, in methanol synthesis.[10] Additionally, monoclinic zirconia has been suggested as a support for water-gas shift reaction catalysts with gold, platinum and copper,[11–13] and for reforming with platinum, nickel, cobalt and copper.[14,15]

Since 2006, monoclinic zirconia has been prepared also in nanoshapes, including nanorods[16,17] and nanosheets.[16] Using the nanoshapes in catalysis might be beneficial due to their well-defined surface sites; thus their selectivities might be more easily linked to the exposed surfaces than those of traditional catalysts in polycrystalline form.

Carbon monoxide interacts with monoclinic zirconia both on a clean surface with few or no hydroxyls,[18] as well as on a hydroxylated surface.[19,20] The surface hydroxyl groups seem to play an important role in the interaction of CO with zirconia as sites for the formation of formates[5,7,20–23] and bicarbonates[22,24–26] but also for inhibiting the formation of adsorbed linear CO species.[27] The main adsorbed CO species are linearly adsorbed CO at room temperature and below and formate species formed above 100 °C, the first one desorbing reversibly[27] and the second one decomposing both reversibly back to gas-phase CO and irreversibly to CO_2 and H_2.[20,21,28]

The interaction of carbon monoxide with zirconium oxide has been studied actively since the 1970s.[5,18,21,23,29,30] Due to differences in zirconia materials and their pretreatments, experimental setups and conditions, the interpretation and comparison of the obtained results are not straightforward. Most of the studies on the interaction with CO have been carried out using infrared spectroscopy.[5,18,19,22–24] However, studies using other techniques, such as temperature-programmed methods,[20,21,28,30] calorimetry,[27,31,32] and gravimetry,[33,34] as well as theoretical studies[22,28] have been published.

The focus of this work is on the monoclinic polymorph of zirconia instead of the whole spectrum of zirconia materials such as doped (including sulphated), tetragonal and cubic zirconia, to name the most significant zirconias excluded from this review. This choice is made for simplicity and

[a] *Department of Biotechnology and Chemical Technology, Aalto University School of Chemical Technology, P.O. Box 16100, 00076 Aalto, Finland. E-mail: sonja.kouva@aalto.fi*
[b] *Department of Chemistry, Nanoscience Center, University of Jyväskylä, P.O. Box 35, 40014 Jyväskylä, Finland*
[c] *Faculty of Science & Technology, University of Twente, P.O. Box 217, 7500 AE Enschede, The Netherlands*

This journal is © The Royal Society of Chemistry 2015

Catal. Sci. Technol., 2015, **5**, 3473–3490 | 3473

clarity, as monoclinic and tetragonal zirconias differ in, *e.g.*, surface hydroxyl species[7,25] and acidity/basicity,[7,24,30] which is further demonstrated in their interactions with CO[7,25,30] and catalytic activity, *e.g.*, in water-gas shift reaction.[11,12] More information can also be found in the reviews by Dyrek

et al.[35] and Hadjiivanov.[36] Most of the pre-1993 studies included in this paper were reviewed 20 years ago by Nawrocki *et al.*[37] in the context of chromatography; this review provides an update, with studies reported since 1993, from the perspective of catalysis.

Table 1 Origin, preparation conditions and surface area of the zirconia samples[a]

Material	T_{calc} (°C)	Atmosphere	A_s (m^2 g^{-1})	Ref.
Decomposition of $ZrO(NO_3)_2 \cdot xH_2O$	300 & 300	Air & 10% H_2	20	42, 43
Hydrolysis of $ZrOCl_2$	600	Air, 4 h	—	9
Hydrolysis of $ZrOCl_2$	300 & 700	O_2, 5 h	110 & 19	25, 30
Hydrolysis of $ZrOCl_2$	700 & 300–550	Calc. & vacuum, air (1 h), H_2, vacuum	44	29
Hydrolysis of $ZrOCl_2$	800 & 1000	Vacuum, 10 min & air, 6 h	—	46
Hydrolysis of $ZrO(NO_3)_2$	500 & 800	Air, 5 h & vacuum, 5 h	—	47
Hydrolysis of $ZrO(NO_3)_2$	700 & 500 & 700	Calc., 3 h & O_2, 10 h & vac., 20 min	58^c	48
Hydrolysis of $ZrO(NO_3)_2$	500 & 500 & 730	Calc., 3 h & O_2, overnight & vac., 20 min	—	49
Hydrolysis of $ZrO(NO_3)_2$	530/710	Air, 3 h	70/58	26
Hydrolysis of Zr isopropylate	447	Calcination	81^c	50
Hydrolysis of Zr isopropylate	447 & 597	Calcination & vacuum, 2 h	82	18
	447 & 27–397	Calcination & vacuum, 2 h	92 (397 °C)	18
Hydrolysis of Zr isopropylate	447 & 797	Calc. & vac., 2 h + 50 Torr O_2, 30 min	36	27
	447 & 397–597	Calc. & vac., 2 h + 50 Torr O_2, 30 min	80–90	27
Hydrolysis of Zr isopropylate	447 & 400 & RT & 250–600	Calc. & vac. + O_2 & H_2O vapor & vac., 2 h	—	38
Hydrolysis of Zr isopropylate	397 & 100–600	Air & vacuum, 2 h + O_2	—	8
Hydrolysis of Zr isopropylate	397 & *e.g.* 597 & *e.g.* 597	Calc. & vacuum, 2 h & O_2, 30 min	—	51
Hydrolysis of Zr isopropylate	597 & 197–597	Calc. & vacuum	78	39
	997 & 197–597	Calc. & vacuum	10	39
Hydrolysis of Zr isopropylate	600/800/900 & 27–800	Air, 3 h & vacuum	55/35/20^c	40
Hydrolysis of Zr isopropylate	400 & 400	Calcination & vacuum	84	52
Hydrolysis of Zr propylate	400	O_2 & vacuum	200–220	53
Hydrolysis of Zr propylate	400	O_2, 1 h & He, 30 min	200	20
Hydrolysis of Zr propylate	440	O_2, 2 h	200–220	54
Hydrolysis of Zr propylate	440	Air, 12 h	120	55
Microemulsion from $ZrOCl_2$	500–1200	Annealing	1.6–44.9	31
NH_3 hydrolysis of $ZrOCl_2$	120 & 400	Drying & preheating	—	56
NH_3 hydrolysis of $ZrOCl_2$	550 & 550	Air, 2 h & N_2, 7 h	70	57
NH_3 hydrolysis of $ZrOCl_2$	550	Air, 1 h	56	58
NH_3 hydrolysis of $ZrOCl_2$	500	Air, 6 h	57	59, 60
NH_3 hydrolysis of $ZrOCl_2$	600	Vacuum	41	7
NH_3 hydrolysis of $ZrOCl_2$	100 & 700	O_2, 5 h	19	41
NH_3 hydrolysis of dissolved $ZrCl_4$	600–900	Air, 2–6 h	8.2–30	45
NH_3 hydrolysis of dissolved $ZrCl_4$	600	O_2	30–36	10
NH_3 hydrolysis of $Zr(NO_3)_4$	500	Air, 2–3 h	80^b	44
PICA process	700	Air, 2 h	33	34
$ZrO(NO_3)_2$ precipitation with hydrazine	1450 & 800	Air & vacuum	1.0	32
A.D. Mackay/nuclear grade	500	Vacuum	23.7	33, 61
Alfa Aesar	>1200 & 800	Air & vacuum	1.6	32
Alfa Aesar	900	Air	10.4	62
Alfa-Ventron	620	O_2, 0.5 h & He, 0.25 h & H_2, 0.5 h	5.8^c	21
Alfa-Ventron	500	O_2, overnight	5.8^c	19
Criceram/$ZrCl_4$ + H_2O vapor	877/903	Air, 24 h/30% O_2 + 70% H_2O, 24 h	6/4.2	63
Daiichi Kigenso Kagaku Kogyo (RC-100)	400	Air, 15 h	71	64
Degussa/flame hydrolysis	600–800	Air or vacuum	37 ± 1^c	65
Degussa	450	Air, 4 h	40	66
Gimex Technical Ceramics (RC-100)	600 & 400	He, 24 h & H_2, 30 min	—	23
Magnesium Elektron (E-10 powder)	—	Vacuum	14	24
MEL EC0100	580	O_2, 2 h	47	22, 67
MEL $Zr(OH)_4$	RT/150/300/500	Vacuum	66.6–537	68
MEL $Zr(OH)_4$	450 & 600	Air, 16 h & O_2/inert, 2 h	90	28
Nanotek	—	—	78	6
Saint-Gobain NorPro	—	—	52	69
Commercial $Zr(OH)_4$	700	Calcination, 6 h	12	70

[a] Tsyganenko *et al.*[3,71] have not reported any details about their zirconium oxide material. [b] Surface area value reported prior to calcination. [c] Surface area value reported prior to wafer pressing.

3474 | *Catal. Sci. Technol.*, 2015, **5**, 3473–3490

This journal is © The Royal Society of Chemistry 2015

2. Preparation, structure, and surfaces

2.1. Preparation

Zirconium oxide can be prepared, *e.g.*, *via* hydrolysis from zirconium isopropylate $(Zr(OCH(CH_3)_2)_4)$[8,18,27,38–40] or zirconium oxychloride $(ZrOCl_2)$,[25,30,41–43] and also from zirconium oxynitrate $(ZrO(NO_3)_2)$[42–44] and zirconium tetrachloride $(ZrCl_4)$.[10,45] Yamaguchi introduces the processes starting from natural ores (zircon $(ZrSiO_4)$, baddeleyite) into zirconium oxide preparation.[2] The origin of the zirconia samples referred to in this review and their preparation conditions and surface areas are presented in Table 1 to aid the reader by presenting the key properties of the materials used. Note that the applied pretreatment conditions might differ from the preparation conditions.

2.2. Crystal structure and surfaces

The unit cell of monoclinic zirconia is face-centered (space group C_{2h}^5), consisting of 4 Zr atoms and 8 O atoms.[72] In the bulk, all Zr atoms are seven-fold coordinated to 3 three-fold coordinated oxygen atoms and 4 four-fold coordinated oxygen atoms.[73] Based on theory, the coordination numbers on the surface differ, *e.g.*, on the ($\bar{1}$11) surface, some of the zirconium atoms are only six-fold coordinated and some of the oxygen atoms are three- or two-fold coordinated instead of four- or three-fold coordinated.[74] On the ($\bar{1}$11) surface, some zirconium atoms can be even five-fold coordinated.[74] The experimentally determined lattice parameters are $a = 5.17$ Å, $b = 5.23$ Å and $c = 5.34$ Å, and the angle is $\gamma = 99.3°$.[75]

Monoclinic zirconia has nine inequivalent crystalline directions altogether: [001], [010], [100], [110], [101], [011], [$\bar{1}$01], [111] and [$\bar{1}$11].[4] Warble reported the (110), (100) and (111) surfaces to be exhibited in transmission electron microscopy (TEM).[76] The (111),[39,40] (001)[39,40] and (011)[40] planes have been reported based on high-resolution TEM (HRTEM) images. Theoretically, the most stable surface of monoclinic zirconia is the ($\bar{1}$11) surface.[4] The difference between the theoretically most stable surfaces and the experimentally observed surfaces might be due to inaccuracy in either method, and it is not clear whether the particle size or, *e.g.*, the degree of surface hydration plays a role. In the nanocrystals, the (011) surface seems to be the most abundant according to TEM, while ($\bar{1}$11), (111) and (001) surfaces have also been observed.[77] The ideal (111), ($\bar{1}$11), (001) and (011) surfaces are shown in Fig. 1. The atom positions are those of the bulk structure, assuming that no reconstruction takes place.

Jung *et al.* reported that the crystallographic structure of zirconia, instead of crystallite size or calcination temperature, is the most significant factor for determining the nature and density of the surface sites suitable for CO_2 and NH_3 adsorption, *i.e.*, the basic and acidic surface sites.[41] Monoclinic zirconia has a higher CO adsorption capacity than tetragonal ZrO_2, which is attributed to its higher Lewis acidity and basicity.[30] The tetragonal structure is more symmetrical than the monoclinic one,[4] leading to a lower number of
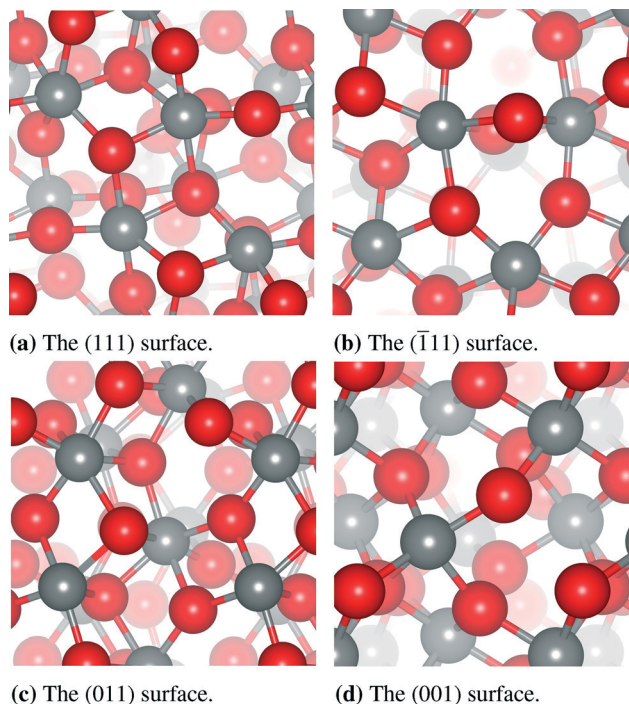

(a) The (111) surface.

(b) The ($\bar{1}$11) surface.

(c) The (011) surface.

(d) The (001) surface.

Fig. 1 Ideal surfaces of monoclinic ZrO_2 (top view); Zr atoms are grey and O atoms are red. The atoms further in the lattice are shaded lighter than those on the surface. The surfaces were visualized using VESTA software.[78]

different surfaces and thus possibly also to less versatile surface site types.

Thermal treatment tends to increase the crystal size of monoclinic zirconia. Increasing the calcination temperature by 300–500 °C can lead to a particle size of three or even four times the original.[40,64] Auger electron spectroscopy (AES)[79] shows that the surface O/Zr ratio decreases from the stoichiometric 2 down to 1.1 with evacuation at 427 °C and 727 °C, respectively. The surface reduction is very fast, and extending the time to one hour in ultra-high vacuum (UHV) does not affect the surface.[79] With H_2, the surface seems unreducible even at 900 Torr and 900 °C while atomic hydrogen already reduces the surface at 750 °C and an H_2 pressure of 5 μTorr prior to atomization.[80] The ineffectiveness of H_2 compared to UHV in surface reduction is rather unexpected, yet atomic hydrogen seems to be a better reductant than molecular hydrogen. Based on the literature, the mechanism for oxygen removal remains unclear; is it removed as O_2 or perhaps through dehydroxylation *via* multicoordinated OH groups, as shown in eqn (1)?

$$\text{multi-OH} + \text{multi-OH} \longleftrightarrow O_{lattice} + \text{vacancy} + H_2O \qquad (1)$$

The presence of Zr^{3+} sites has been proposed based on electron paramagnetic resonance (EPR).[8,46,51,57] The Zr surface cations have been probed with N_2O, which already decomposes on Zr^{3+} at room temperature and also at higher temperatures, and reversibly adsorbs on Zr^{4+} sites.[6] Vacuum

This journal is © The Royal Society of Chemistry 2015

Catal. Sci. Technol., 2015, **5**, 3473–3490 | **3475**

treatment at above 600 °C is sufficient to initiate the formation of oxygen vacancies[81] and reduction of cations from Zr^{4+} to Zr^{3+}.[6,81] Hydrogen treatment at 700 °C also allows transformation of some of the Zr^{4+} sites to Zr^{3+} sites,[81] but with hydrogen treatment at 600 °C, the amount of Zr^{3+} sites does not increase,[9] which is in agreement with the low reducibility with H_2 mentioned previously. If the sample has been vacuum-activated at 400 °C, hydration quenches the defect centers (Zr^{3+}) and the defects would have to be re-created with evacuation.[8] If the sample has been vacuum-activated at 800 °C, there are two options: (1) the defect centers are quenched but they are easier to re-create on a sintered surface, or (2) the defect centers are not quenched, but rather coordinatively saturated with water and dehydration restores their coordinatively unsaturated state.[8] Based on EPR, the most exposed Zr^{3+} sites are transformed to Zr^{4+} when in contact with water (200 °C, 18 Torr H_2O) but the others are coordinatively saturated with water and remaining Zr^{3+}.[8]

Syzgantseva et al. have calculated the formation energies of oxygen vacancies, and based on those, the zirconia ($\bar{1}11$) surface is less reducible than the ($\bar{1}01$) surface,[82] in line with the stability observation by Christensen and Carter.[4] When compared to that of other oxides, the oxygen vacancy formation energy on the zirconia surface is 820–880 kJ mol^{-1} and that in the bulk is ca. 860 kJ mol^{-1}, whereas those for titania, which is considered a reducible oxide, are 530–580 kJ mol^{-1} on the surface and 670 kJ mol^{-1} in the bulk.[82] Syzgantseva et al. have also predicted the conditions necessary to create oxygen vacancies by surface hydrogenation followed by desorption of water (temperature above 927 °C and H_2O/H_2 pressure ratio below 10^{-5}).[82] They concluded that water desorption takes place already under milder conditions, thus simplification in their computations required for, e.g., surface models might cause the discrepancy between theory and experiments.[82]

The oxygen mobility, dissociation and recombination on zirconia among other oxide materials were probed by Martin and Duprez.[66] Isotopic oxygen exchange experiments between $^{16}O_2$ and $^{18}O_2$ showed surface oxygen exchange at 380–780 °C.[66] The maximum O-exchange rate was at 530 °C and the exchange rate was further expedited in the presence of Rh or Pt on the surface.[66] The exchange is attributed to c.u.s. Zr^{3+} centers created by vacuum thermal treatment and their ability to dissociate molecular oxygen.[66] The number of exchanged oxygens on ZrO_2 was found to be greater than the theoretical number of surface oxygen species, implying that bulk oxygen atoms participated in the exchange.[66]

3. Hydroxyl species and the interaction of water and hydrogen on monoclinic zirconia

Dissociative adsorption of water on monoclinic zirconia is exothermic, occurring already at room temperature.[31,69] Therefore, the surfaces of zirconia are hydroxylated under ambient and in most reactive atmospheres. In this section, different types of OH groups are discussed, followed by methods of manipulating the hydroxyl species on the surface of zirconia.

3.1. Nature, density and probing of hydroxyl species

Typical hydroxyl sites reported on monoclinic zirconia include terminal OH groups (also known as mono-coordinated OH) and tribridged OH groups, first assigned by Tsyganenko and Filimonov as a part of a wider study on different oxides including cerium, hafnium, magnesium, nickel, cobalt and several other oxides.[3,71] Schematic drawings of the hydroxyl groups are presented in Fig. 2. The latter species have been assigned as either tribridged[7,25,70,71] or bibridged,[29,53,61,63] or simply presumed as multicoordinated OH groups.[18,19,23,59] In this work, the term multicoordinated is generally used to refer to these species.

The terminal and multicoordinated hydroxyl species are usually observed in IR spectroscopy at 3780–3760 cm^{-1} and 3690–3650 cm^{-1}, respectively,[7,19,50,61,71] as shown in Table 2 and Fig. 3. Jacob et al. assigned the bands to OH groups related to trigonally coordinated O^{2-} anions (ca. 3774 cm^{-1}) and tetrahedrally coordinated O^{2-} anions (ca. 3668 cm^{-1}),[65] however, without further evidence. Yamaguchi et al. suggested that the bands at 3780 cm^{-1} and 3680 cm^{-1} are attributed to isolated hydroxyls (as opposed to hydrogen-bonded ones) of the bridged and terminal type, adapting the interpretation for rutile, a type of TiO_2.[59] The occurrence of a band at 3740–3720 cm^{-1} is typically interpreted as a sign of a tetragonal phase and its bibridged hydroxyl. Yet, the band of terminal OH (typically at 3780–3760 cm^{-1}) shifts towards lower wavenumbers (even down to 3680 cm^{-1}) with increasing degree of hydration due to hydrogen bonding[18] and at this point, the multicoordinated OH band is even below 3600 cm^{-1},[40] as suggested already by Tret'yakov et al.[44] Thus, interpretation of the hydroxyl band position must be done carefully, considering the possibility of hydrogen bonding at higher degrees of hydration. Tsyganenko and Filimonov also reported an IR band at 3380 cm^{-1}, assigned to hydrogen-bonded hydroxyl groups.[3,71] Unresolved broad bands at 3600–2800 cm^{-1} are assigned to hydrogen-bonded polynuclear water species[61] based on the IR spectra of hydrogen bonding of water.[83] The hydrogen bonding is suggested to occur between molecularly adsorbed water and the hydroxyl groups.[18,33,42,53] The OH wavenumber and thermal stability

Fig. 2 Terminal and tribridged hydroxyl species.

3476 | Catal. Sci. Technol., 2015, 5, 3473–3490

This journal is © The Royal Society of Chemistry 2015

Table 2 Experimentally and theoretically determined ν(OH) wavenumbers

Terminal (cm^{-1})	Bibridged (cm^{-1})	Tribridged (cm^{-1})	H-bonded (cm^{-1})	Ref.
Experimental				
3770		3670	3380	3, 71
3776		3667		50
3772		3681 & 3660		7
3775		3675–3668	3600–2800	27
≈3775		3695–3662	<3600	40
3778		3680–3675	3455–3450	63
3779–3771	3738–3727	3682–3660	≈3400	29
3740		3675		19
3760		3660	3600–2800	61
3770		3680		53
3769				24
3774		3668		65, 81
Theoretical				
3822–3743	3755–3568	3647–3498		67
3778	3550	3475		84
	3750	3700		74
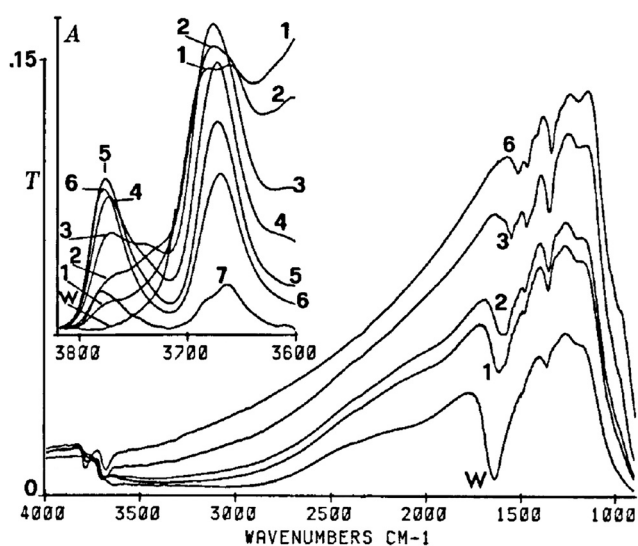
Fig. 3 The evolution of hydroxyl species upon activation after rehydration. Activation conditions: W: rehydrated sample still in 4 Torr of H$_2$O; 1: 27 °C, 5 min; 2: 27 °C, 30 min; 3: 137 °C, 30 min; 4: 247 °C; 5: 327 °C; 6: 397 °C; 7: 497 °C. Reproduced from ref. 18 with permission. Copyright 1988, Elsevier.

depend on the crystalline phase of zirconia;[9] thus, impurities in the crystalline phase can lead to misinterpretation.

Terminal hydroxyls are bound directly to a single cation at oxygen lattice sites; whereas, multicoordinated hydroxyls are located at low-index faces.[61] The former are able to accommodate a water molecule to hydrogen-bond on an edge or a corner site of an oxide particle while the latter are incapable of hydrogen bonding due to steric factors.[61] The assignment of multicoordinated hydroxyls to low-index faces[61] and the observed decrease in the relative amount of terminal OH species upon vacuum treatment at 500–1000 °C[65] are in line with the observation that the regularity of sintered crystals is higher.[39]

Based on IR spectroscopy, the tribridged OH species (at 3690–3681 cm^{-1} and at 3670–3660 cm^{-1}) on zirconia are suggested to be actually two species,[7,40] and signs of multiple tribridged species are also seen at both high[18,28] and low[18] degrees of hydration. The OH species differ slightly in their acidic character[40] and their behavior upon calcination at 600–900 °C suggests that the low-frequency band (3670–3660 cm^{-1}) should be assigned to tribridged species at crystallographic defects selectively annealed during sintering.[40] However, in our recent investigations on reduced zirconia with no visible H-bonding effect, both terminal and multicoordinated bands shift towards lower wavenumber with increasing temperature.[28]

The nature of the multicoordinated OH species has also been considered at the atomic level. The ZrO$_2$ (111) surface is suggested to have too small a distance between the c.u.s. O^{2-} and c.u.s. Zr^{4+} sites (only 2 Å),[40] which is not enough space to dissociate a water molecule to form terminal and bibridged OH groups. The corresponding distance between Zr^{4+} and tribridged oxygen is ≈2.3 Å, allowing the formation of terminal and tribridged hydroxyls via dissociation.[40] Based on theory, both bibridged and tribridged species exist.[67,74] Korhonen et al. reported that at low coverage (θ = 0.25 ML), there are only bibridged hydroxyls on the ($\bar{1}$11) and ($\bar{1}$01) surfaces.[67] Bibridged hydroxyls are also claimed to form following dissociative adsorption on the (001) surface until full coverage (θ = 1 ML) is obtained.[85]

Hydroxyl IR vibrations have been determined computationally[67,74,84] as shown in Table 2. A large variation of calculated frequencies which span, e.g., over 200 wavenumbers for tribridged OH species has been demonstrated. The diversity of calculated frequencies for adsorbed OH is not unique to ZrO$_2$ as it is also reported for CeO$_2$.[86] The overall discrepancy between calculated and experimental frequencies can be derived from three different origins. Firstly, frequencies are typically calculated using a so-called harmonic approximation, which specifically leaves out possible anharmonic effects leading, in part, to errors in calculated frequencies. Secondly, discrepancies can also originate from the inability of density functional theory (DFT) to reliably describe the electronic structure of a given system. Thirdly, for polycrystalline oxide nanostructures, the discrepancy between calculated frequencies and experimental ones can stem from the fact that an active surface site cannot experimentally be identified definitely. This may lead to an inaccurate computational adsorption site model, which differs from the real adsorption site. Moreover, the application of a cluster model to simulate ZrO$_2$ surfaces can impact on the calculated frequencies.

Hydroxyl densities can be estimated based on the amount of water removed from zirconia[34] and water adsorbed on zirconia,[27,69] or quantification via ^{1}H MAS NMR,[68] and these estimates are presented in Table 3. In the table, the scaled values represent OH densities regardless whether it has been measured directly or by water adsorption (each water molecule is assumed to form two surface hydroxyls).

This journal is © The Royal Society of Chemistry 2015

Catal. Sci. Technol., 2015, 5, 3473–3490 | 3477

Table 3 Hydroxyl densities reported in the literature

Measurement	As reported	Scaled to μmol_{OH} m^{-2}	Ref.
OH concentration (SA = 19 m^2 g^{-1})	6.2 OH per nm^2	10.30	25
OH concentration (SA = 110 m^2 g^{-1})	9.4 OH per nm^2	15.61	25
Induced hydroxyls (desorbed above 200 °C) after 48 h in humid N$_2$ at RT	20.2 μmol_{OH} m^{-2}	20.2	34
OH coverage calc. from H$_2$ evolution after standardization (400 °C, O$_2$, 1 h)	2.1 × 10^{13} OH per cm^2	0.35	20
Estimated full OH coverage before standardization	7.2 × 10^{13} OH per cm^2	1.2	20
Estimated chemisorption capacity at 25 °C	5.7 mg$_{H_2O}$ g^{-1}	26.7	33
Irreversibly adsorbed water at 25 °C	4.8 mg$_{H_2O}$ g^{-1}	22.5	33
Surface hydrogen after H$_2$O adsorption at 200 °C	4.20 H per nm^2	6.97	69
Surface hydrogen after H$_2$O adsorption at 300 °C	3.62 H per nm^2	6.01	69
Surface hydrogen after H$_2$O adsorption at 400 °C	3.22 H per nm^2	5.51	69
Full coverage of water (2× half-layer coverage)	4.4 H$_2$O per nm^2	14.6	31
Theoretical H$_2$O adsorption capacity at θ = 1 ML on ($\bar{1}$11) surface	8.9 H$_2$O per nm^2	29.6	77
Theoretical H$_2$O adsorption capacity at θ = 1 ML on (111) surface	7.1 H$_2$O per nm^2	23.6	77
Theoretical H$_2$O adsorption capacity at θ = 1 ML on (011) surface	5.2 H$_2$O per nm^2	17.3	77
Theoretical H$_2$O adsorption capacity at θ = 1 ML on (001) surface	7.5 H$_2$O per nm^2	24.9	77

The observed amount of adsorbed water decreases with increasing temperature, as expected. Based on an estimated number of Zr atoms on the ZrO$_2$ surface (*ca.* 12 μmol m^{-2}) and water adsorption leading to formation of two OH groups, one on a Zr cation and one on a surface oxygen, the estimated hydroxyl densities seem reasonable in magnitude. Nawrocki *et al.* reported a theoretical maximum OH concentration of *ca.* 25 μmol m^{-2} based on the average surface Zr concentration of *ca.* 12.2 μmol m^{-2}.[37] The amount of induced hydroxyls (20.2 μmol m^{-2} desorbed above 200 °C)[34] seems to be in agreement with the estimated total OH capacity. Piskorz *et al.*[77] have also reported similar theoretical OH site densities.

The energetics of water adsorption has been investigated with both experimental and theoretical approaches. Piskorz *et al.* have studied the effect of surface hydration on the stability of crystal planes using DFT calculations.[77] A hydroxylated surface is favored over a clean surface on very small crystallites (<20 Å), whereas hydration does not enhance the stability of the surface on crystallites between 500 Å and 2000 Å, and the authors claimed that the transformation from clean to hydrated surface is attenuated.[77] However, this is not in line with experimental observations suggesting the hydroxylated surface to be the prevalent one. Based on microcalorimetry, the integral enthalpy of adsorption for a half-layer coverage of water (3.65 μmol m^{-2}) is −142 kJ mol^{-1} on monoclinic ZrO$_2$ nanoparticles (crystal size of 100–500 Å, specific surface area of 1.6–27.2 m^2 g^{-1}).[31] This is in agreement with the values measured for powder zirconias (1.0–1.6 m^2 g^{-1}),[32] giving a range from −110 kJ mol^{-1} to −170 kJ mol^{-1}. Theoretical adsorption energy values typically range from −80 kJ mol^{-1} to −190 kJ mol^{-1} on (001), ($\bar{1}$11), (111), and ($\bar{1}$01) surfaces.[67,69,85] We have recently reported the dissociative adsorption energies of the first adsorbed water molecule ranging from −106 to −119 kJ mol^{-1} up to −297 kJ mol^{-1} for flat, stepped and corner adsorption sites.[28] The calculated values demonstrate the structure sensitivity of dissociative adsorption of water, which is clearly most

favorable on a c.u.s. site such as a corner site as suggested by our DFT calculations.[28]

3.2. Manipulation of hydroxyl species

The intensity ratio of terminal and multicoordinated hydroxyls varies according to temperature, used atmosphere and pretreatment. Hydroxyl species can be added to the surface with water or hydrogen treatment and removed using heat together with inert gas or evacuation. The initial state of zirconia can usually be restored by evacuation or flushing with inert gas at the same temperature as before rehydration.[28,53]

Sample hydration is typically carried out by adsorption of water vapor, either by letting the sample adsorb moisture from air (virgin material in ref. 18), equilibrating in a closed vessel with water vapor in nitrogen (to avoid CO$_2$ adsorption),[34] or by feeding water vapor into the sample.[18,23,28,58,65] The rehydrated sample can be used as such or after further dehydration with vacuum and/or elevated temperature (*e.g.* ref. 18 and 65). Rehydration has also been carried out by exposing the sample to hydrogen at room temperature[53] or by letting the zirconia sample to be in contact with water-saturated hydrogen for 10 min at 50 °C.[42] Unfortunately, rehydration is often described vaguely, omitting time, water vapor concentration or temperature, which are all relevant in controlling the degree of hydroxylation.

The commonly used methods for dehydration are vacuuming[20,24,33,70] or flushing[67] at elevated temperatures. Undissociated water adsorbed at room temperature is completely removed in vacuum at 127 °C[27] and after evacuation at 200 °C, only two distinct OH bands at *ca.* 3775 cm^{-1} and 3665 cm^{-1} remain.[40] Köck *et al.* pretreated zirconia in air at 900 °C to completely dehydroxylate the sample, and only very weak OH bands remained.[62] Evacuation at 500 °C is reported to be insufficient for complete dehydroxylation,[20] but at 550 °C, spectra with no trace of surface hydroxyls after evacuation are shown.[53] The conditions

3478 | *Catal. Sci. Technol.*, 2015, **5**, 3473–3490

This journal is © The Royal Society of Chemistry 2015

necessary for total OH removal are at *ca.* 550–750 °C *in vacuo*,[18,44,65] in agreement with the enthalpies for water adsorption discussed earlier in this paper in Section 3.1. As most pretreatments and processes do not reach these conditions, the presence of these OH groups on the zirconia surface in such processes is practically inevitable, especially in biomass-based processes, where water is present.

The partial dehydration method[18,44,53,65] can be used to vary the concentration of several types of OH groups on zirconia. Depending on whether the amount of adsorbed water results from dehydration or rehydration, the surface species distribution might be different as demonstrated by Bolis *et al.*[27] through heating a sample in a closed vessel and analyzing the OH distribution on the sample before and after heating. Based on their findings, dehydration is systematic even in terms of surface effects whereas rehydration is more irregular as water collides and dissociates on the surface as hydrogen-bonded pairs.[27] Thus, allowing the system to approach equilibrium leads to a more even surface distribution. All in all, the method chosen to adjust the amount of hydroxyls influences their distribution on the zirconia surface.

Cerrato *et al.* suggested based on theory that water dissociates to form a tribridged OH at a tricoordinated c.u.s. oxygen and a terminal OH on a c.u.s. cation, leaving a monocoordinated c.u.s. oxygen in the same sphere unsaturated.[40] The presence of the suggested monocoordinated c.u.s. oxygen is in agreement with CO_2 adsorption experiments on a fully hydrated surface, yielding monodentate and bidentate carbonate species requiring the presence of basic, c.u.s. oxygen ions.[40]

Based on theory, dissociative adsorption of the first adsorbed water molecule of a unit cell ($\theta = 0$–0.25 ML) has been reported on ($\bar{1}11$),[67,77] ($\bar{1}01$),[67] and (111)[77] surfaces. The second H_2O molecule adsorbs molecularly on ($\bar{1}11$)[67,77] and (111)[77] surfaces, and dissociatively on ($\bar{1}01$)[67] surfaces. The additional H_2O molecules adsorb molecularly.[67,77] For both ($\bar{1}11$) and ($\bar{1}01$) surfaces, the first water molecule forming two hydroxyls is already hydrogen-bonded.[67] Iskandarova *et al.* have reported both dissociative and molecular adsorption enthalpies resulting in coverages of 0.5 ML and 1 ML on a (001) surface, in which dissociative adsorption is favored by 45–75 kJ mol^{-1} in both cases.[85] Our recent investigations suggest that at $\theta = 0.25$ ML, hydrogen bonding exists between the hydroxyl groups on the ($\bar{1}11$) surface but not on the hydroxylated ($\bar{2}12$) edge and corner sites.[28] Cerrato *et al.* pointed out that hydrogen bonding at high hydroxyl coverages only takes place between OH species and coordinated undissociated water whereas hydrogen bonding between OH pairs is unlikely to occur.[40]

Morterra *et al.* hypothesized that if all surface oxygens on a (111) surface are transformed into hydroxyls to maintain electrical neutrality, and then dehydration takes place *via* desorption of terminal hydroxyls and hydrogen atoms from bridging OH groups (shown in Fig. 4), only bridging oxygens are left behind, and thus highly uncoordinated Zr^{4+} sites are achieved.[39] The decrease in intensity of the terminal hydroxyl species is greater than that of multicoordinated OH when the
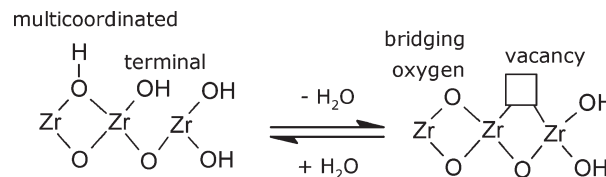

Fig. 4 (De)hydroxylation mechanism.

zirconia sample is thermoevacuated at 500–600 °C after calcination at 600 °C.[70] Dehydration in vacuum at 500–1000 °C followed by hydration caused the relative amount of terminal OH to decrease significantly compared to that of multicoordinated OH, whereas oxygen treatment (500–750 °C) before hydration had the opposite effect.[65] The decrease in terminal hydroxyls by high-temperature vacuum treatment is assigned to an increasing amount of tetragonal zirconia, as the tetragonal phase is stabilized by oxygen vacancies.[65]

One approach for hydroxyl studies is to replace hydrogen with its heavier isotope deuterium using D_2 or D_2O, or to replace ^{16}O with ^{18}O, all of which are easily observable in both IR and mass spectrometry. OD groups, known as deuteroxyls, have been investigated by many groups[19,21,24,42,44,56,59,61,87] while oxygen-labeling studies are scarcer.[66,69,81]

Observed deuteroxyl IR wavenumbers are collected in Table 4. Erkelens *et al.* reported that the ratios of the frequencies between the OH bands (3732 cm^{-1}, 3660 cm^{-1} and 3584 cm^{-1}) and the OD bands (2758 cm^{-1}, 2702 cm^{-1} and 2651 cm^{-1}) are *ca.* 1.36, in agreement with the expected isotopic substitution.[56] Similar results with an additional OH band at 3738–3727 cm^{-1} (OD at 2757–2748 cm^{-1}) were reported also by Guglielminotti.[29] A spectrum showing the changes in OH/OD groups is shown in Fig. 5.

Repeated treatments with, *e.g.*, 10 Torr of D_2O vapor[44] at room temperature almost completely replace hydrogen with deuterium in both terminal and multicoordinated OH, resulting in corresponding OD groups.[19,24,44,56,59,61] The terminal species seem to exchange more easily than the multicoordinated species.[24,59]

Ignatchenko *et al.* proposed that the hydrogen–deuterium exchange mechanism would proceed *via* hydroxyl/deuteroxyl exchange so that deuterated water adsorbs adjacent to an existing terminal hydroxyl species and a hydrogen bond is formed between the D_2O and OH species.[69] Then, the hydrogen-bonding deuterium atom and the original OH

Table 4 Experimentally determined ν(OD) wavenumbers

Terminal (cm^{-1})	Multicoordinated (cm^{-1})	Other (cm^{-1})	Ref.
2780	2703		44
2758	2702	2651	56
2770	2695		61
2785–2779	2713–2701	2757–2748	29
2780	2710		59
2783	2713–2710		63
2760	2706		48
2760	2710		19
2782	2705		81

This journal is © The Royal Society of Chemistry 2015

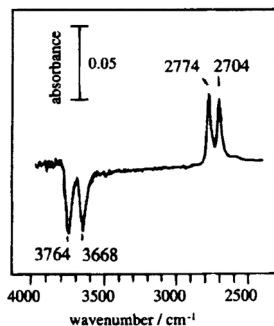*Catal. Sci. Technol.*, 2015, **5**, 3473–3490 | **3479**

Fig. 5 Difference spectra of OH/OD species before and after 30 min in 100 Torr of D_2 at 150 °C. Reproduced from ref. 87.

group desorb as HDO species, leaving the OD species on the surface. The mechanism is shown in Fig. 6.

Labeling the oxygen of water ($H_2^{18}O$) reveals that the oxygens of hydroxyls are thoroughly exchanged at 400 °C, yet at 200 °C, the findings of Ignatchenko et al.[69] disagree with the suggested mechanism in Fig. 6. It appears that at 200 °C, the terminal hydroxyls can be exchanged already but for the multicoordinated ones, higher temperatures (closer to 400 °C) are required,[69] and the presented mechanism should be modified so that it can also be applied to multicoordinated hydroxyls. Based on these findings, it seems that hydrogen scrambling follows the suggested mechanism[69] (see Fig. 6). The terminal OH species are completely exchanged via the normal (de)hydroxylation mechanism involving also multicoordinated OH groups and labeled $H_2^{18}O$, as deduced from the applied temperature range (200–400 °C). The exchange of multicoordinated hydroxyls requires a new mechanism hypothesis and we propose that multi-OH groups are removed as water, leaving behind one oxygen atom and an oxygen vacancy (see eqn (1)). This mechanism may be predominant only at high temperatures when terminal OH species have already been desorbed.

In addition to water or its deuterated counterpart, H_2 or D_2 can also be used to create surface OH or OD groups on monoclinic zirconia. He and Ekerdt have suggested that gas-phase hydrogen is able to replenish OH groups,[21] with the hydroxyl IR bands emerging at 200–600 °C[9,48,53] for both terminal and multicoordinated hydroxyl species.[53]

The mechanism for hydroxyl formation by molecular hydrogen can be either homolytic, resulting in two hydroxyl species and two electrons,[9] or heterolytic, resulting in IR-inactive Zr–H (H^+ type) species and a hydroxyl (OH) species.[49] At temperatures above 100 °C, large amounts of hydroxyl
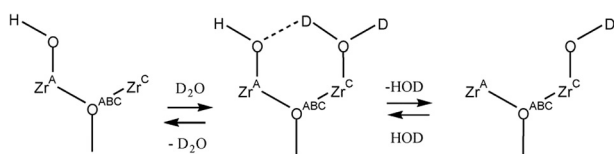
species are formed likely due to homolytic dissociation of hydrogen,[48] whereas hydrogen contact at room temperature induces heterolytic dissociation.[48] Heterolytic dissociative adsorption of H_2 at room temperature seems to require unhydroxylated c.u.s. Zr sites, as pretreatment above 600 °C is necessary to remove adsorbed water from the zirconia surface.[26,49] Even though Bianchi et al. have observed increasing hydroxyl species IR intensities during H_2 treatment, they reported that no adsorption or desorption of hydrogen at 25–400 °C, and no water evolution during H_2-TPR from 25 °C up to 700 °C occur.[53] Assuming that no redox process concerning the Zr cations takes place, a hydrogen desorption mechanism is postulated for Zr–H and Zr–OH sites leading to Zr and Zr–O sites, as hydrogen adsorbed at 550 °C is desorbed from m-ZrO_2 at 600 °C.[9]

According to Syzgantseva et al., hydrogen dissociates on Zr^{3+} with a neighboring oxygen vacancy (ν_O), leading to formation of Zr–H hydrides and transformation of Zr cations into Zr^{4+} species.[82] The proposed mechanism is presented in Fig. 7. Addition of gas-phase oxygen to Zr–H hydrides, produced by gas-phase H_2 at room temperature, increases the OH intensity at 3668 cm^{-1} (generally considered as multicoordinated OH), generates an OH band at 3774 cm^{-1} (terminal OH) and decreases the intensity of the Zr–H species at 1565 cm^{-1}.[81] Substituting regular oxygen ($^{16}O_2$) with isotopically labeled oxygen ($^{18}O_2$) does not affect the position of the OH bands (expected shift of 11 cm^{-1}), thus OH formation seems to occur on lattice oxygen rather than oxygen species originated from the gas phase.[81]

Treatment with deuterium gas at 200 °C (1 h, 18 Torr) and 250 °C (1 h, 250 Torr) is sufficient to exchange virtually all hydrogen of hydroxyl groups to deuterium.[56] He and Ekerdt reported that the deuterium in OD groups is replaced already with hydrogen at 200 °C with hydrogen dissociating on the zirconia surface.[19] At 150 °C and in 488 kPa of D_2, half of hydrogen in surface OH species is exchanged to deuterium within 30 seconds.[42] The H/D exchange takes place already at 100 °C with D_2 in the gas phase, however, at 200 °C the exchange rate increases considerably.[26] The activation energies of the H/D exchange reaction with D_2 are similar for both terminal and multicoordinated hydroxyls, and they seem to increase with progression of the reaction.[26] This is interpreted to be due to the overall exchange (migration and replacement of atomic hydrogen with deuterium) being limited by D migration on the surface, subject to heterogeneity of potential barriers to various sites.[26]

Merle-Méjean et al. have found that on air-calcined zirconia, the hydroxyl species are H/D exchanged upon contact

Fig. 6 The OD exchange mechanism proposed by Ignatchenko et al.[69] Reproduced from ref. 69 with permission. Copyright 2006, Elsevier.

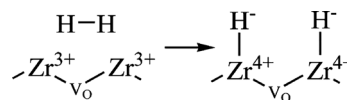

Fig. 7 The hydrogen dissociation mechanism proposed by Syzgantseva et al.[82] Reproduced from ref. 82 with permission. Copyright 2012, American Chemical Society.

with D_2 (507 °C, 100 hPa) so quickly that it gives reason to believe that the OH species are on the surface only.[63] Conversely, on steam-calcined zirconia, some hydroxyls are exchanged to deuterium-containing species so slowly (during several hours), if at all, that they must be elsewhere in the oxide, likely in the bulk.[63]

The presence of formate species is suggested to decrease the number of available sites for H_2/D_2 dissociation as well as partially block the path for surface transport of H or D atoms.[42] If there are formates on the surface, the H/D exchange between OH and OD species at 150 °C is 4–36 times slower depending on the formate coverage (0.3 or 0.8 times the maximum coverage).[42] The overall extent of the H/D exchange of multicoordinated OH to OD is limited to 9% with formate and 2% with methoxy species as compared to that in the normal ZrO_2 surface.[26]

4. Interaction with CO

Upon contact with monoclinic zirconia, CO tends to form several surface species; at low temperatures up to *ca.* 100 °C, the preferred species is linearly adsorbed CO and, at higher temperatures, the dominating surface species is formate. In addition to these, carbonate and carboxylate-type species have also been observed.

4.1. Linear CO species: formation and stability

CO adsorption at room temperature leads to the formation of linear CO species on cationic sites of the zirconia surface (see Fig. 8), for which the corresponding bands in the IR spectra are located at *ca.* 2200–2170 cm^{-1}.[5,18,48,50] The spectra of linear CO species as a function of CO pressure for two differently prepared samples are shown in Fig. 9. The presence of a weak band at 2112 cm^{-1} is reported after CO adsorption at room temperature.[48] With adsorption below room temperature, *e.g.*, at −173 to −195 °C, the IR bands of adsorbed linear CO species extend to the range *ca.* 2200–2140 cm^{-1} at varying CO pressures (from 10^{-4} to 40 Torr).[39,58]

Morterra *et al.* reported that the linearly adsorbed CO species seen in IR at room temperature are at wavenumbers 2198–2187 cm^{-1} and 2188–2174 cm^{-1}, named as $(CO)_H$ and $(CO)_L$ after the high-frequency and low-frequency bands.[18] Also, Guglielminotti demonstrated that CO has adsorbed on zirconia at room temperature, and his results for either reduced (550 °C) or oxidized (400–550 °C) and vacuum-
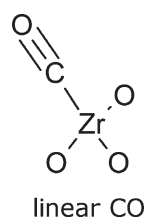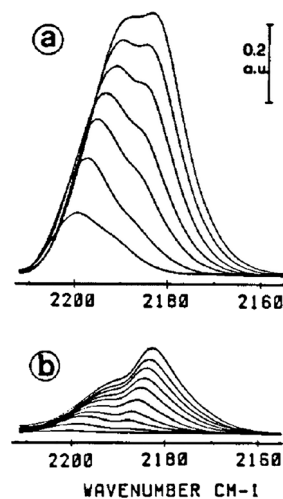

Fig. 9 Spectra of CO adsorbed at room temperature on a ZrO_2 sample calcined at 597 °C (a) and at 997 °C (b), followed by vacuum-activation at 597 °C. P_{CO} = 2 × 10^{-1}–1.2 × 10^2 Torr. Reproduced from ref. 39 with permission. Copyright 1991, Elsevier.

activated (400 °C) samples show strong bands at around 2200 cm^{-1}.[29] For samples reduced at 300 °C and/or vacuum-activated at 500 °C after oxidation, adsorbed CO is observed also at 2110 cm^{-1}.[29]

The IR bands at *ca.* 2200–2190 cm^{-1} are interpreted as CO adsorbed on Zr^{4+},[6,27,29] and the band at *ca.* 2120–2110 cm^{-1} is assigned to CO on Zr^{3+} surface ions;[6,7,9,29,81] ESR (electron spin resonance spectroscopy) results are interpreted so that Zr^{3+} surface ions do not interact with CO at room temperature.[47] The appearance of IR bands assigned to adsorbed CO at wavenumbers higher than that of gas-phase CO (at 2202 cm^{-1}) is attributed to polarization of the CO molecule on the surface.[48] At room temperature, the OH groups are not modified during CO adsorption.[54]

The $(CO)_H$ and $(CO)_L$ species are suggested to be on two types of Lewis-acidic centers,[18] both types assigned as Zr^{4+} ions.[27] For CO chemisorption, these centers are suggested to be caused by differences in crystallography and/or coordinative configurations as the $(CO)_L$ intensity increases while the $(CO)_H$ intensity declines with increasing activation temperature as a result of the initial sintering process.[18] The $(CO)_L$ sites are therefore assigned to flat sites whereas the $(CO)_H$ sites are thought to be on rougher (high-index) planes or structural defects such as steps, kinks, or corners.[27] Sintering the surface indeed causes a sharp relative decline of $(CO)_H$ intensity (at *ca.* 2190 cm^{-1}) in IR, and the sintered surface seems to have more extended and regular flat surface sites based on HRTEM images.[39]

Linear CO is reversibly adsorbed on the surface at room temperature and the removal of CO from gas phase results in the disappearance of its IR band.[20,27,54,55] CO adsorption at room temperature and constant CO pressure shows constant intensity against time-on-stream if measured by the band at *ca.* 2192 cm^{-1},[20,54] indicating unactivated adsorption. Jung

Fig. 8 Linearly adsorbed CO species.

and Bell presented an interesting scheme (see Fig. 10) relating linearly adsorbed CO and its interactions with the zirconia surface.[25] In the scheme, they showed two differently coordinated adsorbed CO molecules with bicarbonate and bidentate carbonate as transformation intermediates; in the former case, the Zr^{4+} cation will have a lower Lewis acidity in the vicinity of an OH group, leading to a lower displacement value of the IR wavenumber compared to that of the gasphase CO IR band, than that with the bidentate carbonate intermediate in a c.u.s. oxygen environment.[25]

Increasing the CO partial pressure increases the adsorbed CO band intensity.[20,52] The intensity ratio of the two adsorbed CO species favors $(CO)_H$ at low coverages and $(CO)_L$ at high CO pressures.[18,27] An increase in the CO partial pressure shifts the IR band position down from *ca.* 2195 cm^{-1} to 2188 cm^{-1},[27,50,52,54] and the overall surface area of the band indicates adsorption according to Langmuir's adsorption model with increasing CO partial pressure.[54]

Increasing the adsorption temperature shifts the main band at *ca.* 2190 cm^{-1} towards higher wavenumbers.[18,55] This shift is attributed to inductive effects, as the charge-release mechanism of adsorbed CO is affected by these, as well as the influence of other surface species (*e.g.* OH) on adsorbed CO.[18] The temperature range with detectable linear CO bands extends typically to *ca.* 100–150 °C,[48,54,55] but it has been reported even at 250 °C[25] at 2184.9 cm^{-1} (CO pressure not reported). Ma *et al.* observed a band at 2109 cm^{-1} during CO adsorption at 350 °C, which is linked to CO adsorption on c.u.s. Zr^{3+}.[7]

The reported linear CO coverages are scaled to μmol m^{-2} and collected in Table 5. The amount of adsorbed CO depends on the adsorption temperature; the coverage at –173 °C is significantly higher than the coverage at room temperature. As can be seen in Table 5, dehydroxylation increases the linear CO adsorption capacity,[20] as dehydroxylated surfaces have a higher number of bare zirconium cations. Increasing the activation temperature results in increasing monolayer capacities for both $(CO)_L$ and $(CO)_H$,[27] as

expected due to lower hydroxyl coverage with increasing activation temperature. It has been estimated that 50% of the dehydroxylated sites can adsorb CO reversibly.[20] The capacity for the $(CO)_H$ species is significantly lower than that for the $(CO)_L$ species, the latter almost four-fold higher compared to the former.[27]

Dulaurent and Bianchi have assumed Langmuir adsorption, calculated adsorption coefficients from IR data and used them with statistical thermodynamics to extract heats of adsorption, and their results range from 55 kJ mol^{-1} to 42 kJ mol^{-1} (at zero and saturation coverage, respectively).[55] The molar heat of adsorption determined by microcalorimetry is reported to be 65–73 ± 2 kJ mol^{-1} for $(CO)_H$ and 44–50 ± 2 kJ mol^{-1} for $(CO)_L$,[27] and that for Lewis-acidic sites at vanishing coverages is *ca.* 60 kJ mol^{-1}. Based on theory, the adsorption energy of linearly adsorbed CO is determined to be –45 kJ mol^{-1}.[28] To give an idea on the strength of CO adsorption on the Zr^{3+} sites, CO on Zr^{4+} (at *ca.* 2200 cm^{-1}) can be removed by evacuation at room temperature and CO on Zr^{3+} (at *ca.* 2110 cm^{-1}) is slightly more strongly bound to the zirconia surface, yet it is also possible to evacuate at room temperature.[29] The observed IR band intensities of the $(CO)_H$ and $(CO)_L$ species with increasing CO pressures are in line with their heats of adsorption; the $(CO)_H$ species with a higher heat of adsorption have a higher intensity at low pressures and *vice versa* at higher pressures.[27]

As shown in Table 5, the linear CO adsorption capacity on dehydroxylated surfaces is higher than that on hydroxylated surfaces. The hydroxyl species have an adverse effect on adsorption of CO as linear CO,[20,27,28] completely suppressing CO adsorption at room temperature already at a surface concentration of 2.4 μmol m^{-2} H$_2$O,[27] corresponding to 20% surface coverage. The more strongly adsorbed linear CO species, $(CO)_H$, seem to be more suppressed than the more weakly adsorbed species when the sample is changed from a dehydroxylated one to one with low OH coverage,[27] suggesting that the site for $(CO)_H$ is the preferred site for hydroxyl formation. Four irreversibly held water molecules are required to eliminate one acidic site based on adsorption capacity experiments at varying degrees of hydration.[27] This 4 : 1 ratio between water and CO suggests that the adsorption sites for linearly adsorbed CO represent only a minority of the sites available for water adsorption. This division is also reflected in the adsorbed amounts of water or OH groups (Table 3) and linearly adsorbed CO (Table 5).

In addition to increasing the adsorption capacities, dehydroxylation seems to shift the bands of the adsorbed CO species towards higher wavenumber; once complete dehydroxylation has been carried out by evacuation at 597 °C, the bands only decrease in intensity, especially the $(CO)_H$ band intensity which decreases as is expected due to the sintering process affecting first the minority sites.[27] Morterra *et al.* indicated that on a highly hydrated surface, local interactions among hydroxyls exceed the adsorbate–adsorbate interactions caused by CO, *i.e.*, the ordered CO oscillator network is interfered with the hydroxyls present.[39]
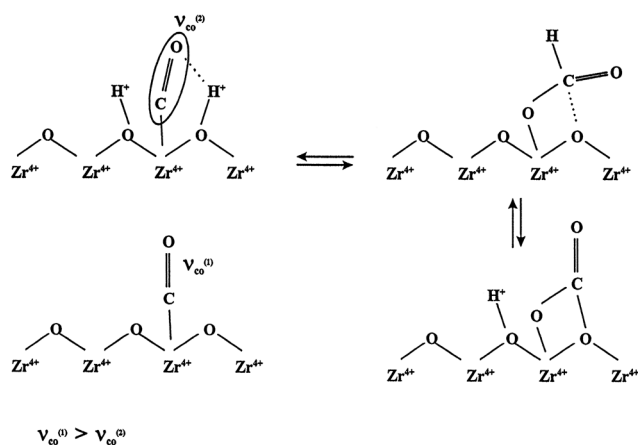

Fig. 10 Interactions of linearly adsorbed CO with the ZrO$_2$ surface. Reproduced from ref. 25 with permission. Copyright 2000, Elsevier.

Table 5 Linear CO coverages reported in the literature

Measurement	As reported	Scaled to $\mu mol\ m^{-2}$	T_{ads}	P_{CO}	Ref.
Adsorbed quantities of CO[a]	Up to 220 $\mu mol\ g^{-1}$	up to 2.7	RT	N/A	50
Monolayer (ML) capacity for $(CO)_H$	0.12–0.24 molec. per nm^2	0.2–0.4	RT	70 or 20 Torr[b]	27
Monolayer (ML) capacity for $(CO)_L$	0.5–0.8 molec. per nm^2	0.8–1.3	RT	N/A[c]	27
Monolayer coverage for CO	0.65 CO sites per nm^2	1.1	RT	60 Torr	52
ML capacity for a fully dehydroxylated sample	1.04 molec. per nm^2	1.73	RT	N/A	27
$Zr^{+\delta}$ sites available for linear CO adsorption	8×10^{13} sites per cm^2	1.33	RT	N/A	55
Total CO coverage on a hydroxylated surface	2.7 molec. per nm^2	4.5	−173 °C	260 Pa	58
Total CO coverage on a dehydroxylated surface	3.8 molec. per nm^2	6.3	−173 °C	260 Pa	58

[a] Assuming full adsorption on the surface from a known amount of fed CO. The IR band in the presence of CO gas at 800 Pa is thrice as intense as the one with 2.7 $\mu mol\ m^{-2}$. [b] Saturation pressure: 70 Torr for samples activated at 397 °C and 597 °C and 20 Torr for the sample activated at 797 °C. [c] Estimated to be 30% higher than the adsorption capacity at 130 Torr.

Morterra *et al.* have looked at CO adsorption on cationic Zr sites after rehydration and they reported that the CO species adsorbed at 2145 cm^{-1} (assigned to CO adsorbed on Zr^{4+} centers *via* σ bonds) are quickly suppressed with water, but the lower wavenumber band tends to shift downwards from 2112 cm^{-1} to 2102 cm^{-1} (proposed to be c.u.s. cationic center Zr^{n+}, where $n < 4$) and increase in intensity.[8] The overall surface coverage of charge-releasing CO species also inductively affects the position of the adsorbed CO band.[8]

Even though hydroxylation decreases the linear CO adsorption capacity,[27,58] surface hydroxyls are important surface sites for adsorption of CO as formate species.[5,21] Linearly adsorbed CO intensities during room-temperature adsorption have been compared before and after CO adsorption at elevated temperature.[54,55] Dulaurent and Bianchi reported that after CO adsorption at 85 °C or 152 °C, cooling to 27 °C and another CO adsorption, the absorbance of the linear CO band is reported to decrease by 12% or 35%, respectively.[55] Mugniery *et al.* showed the spectra where formate pre-adsorption at 300 °C shifts the linear CO bands from 2192 cm^{-1} to 2177 cm^{-1}.[54] When these bands are compared to the spectra obtained by Morterra *et al.*,[38] we note that the $(CO)_H$ species are suppressed by formates, linking the formate and $(CO)_H$ to the same Zr^{4+} surface site. As mentioned earlier, investigation of the CO pressure effect on the band revealed that $(CO)_L$ is the preferred species at high coverages. However, it is not clear whether that applies also to increasing formate coverage (or coverage of any species) or if the $(CO)_H$ site is occupied or otherwise hindered due to the adsorbed formate species.
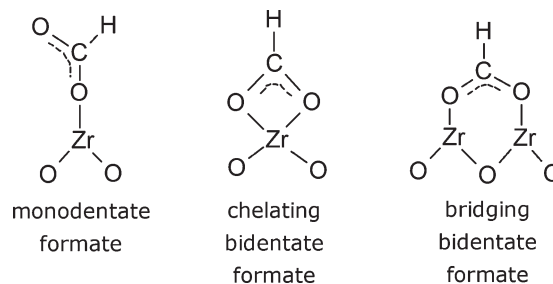
IR bands in Table 6. Unlike linearly adsorbed CO formation, formate formation (see eqn (2)) is an activated process, and its rate expression is shown in eqn (3).

$$CO + OH^* \leftrightarrow COOH^* \qquad (2)$$

$$r_f = k \cdot P_{CO} \cdot [OH^*] \qquad (3)$$

Due to the activated formation process, at low temperatures (*e.g.* $T < 200$ °C), the adsorption time affects the amount of formate formed, whereas at high temperatures, the system quickly reaches equilibrium; however, the equilibrium coverage is also temperature-dependent. The activated nature of the process is demonstrated with increasing intensity of the formate IR bands at different temperatures (25–350 °C) and adsorption times ranging from 30 min up to 18 h.[19,42,54] Formate formation requires rearrangement of at least three bonds, cleavage of the O–H bond, and formation of the O–C and C–H bonds.[28] The theory-based estimate for the activation energy of formate formation is 154 $kJ\ mol^{-1}$,[28] which is in agreement with the experimental observations, yet no experimental value for the activation energy has been reported.

Overall, the observed temperature range for formate species is wide, ranging from *ca.* 85 °C up to 550 °C.[7,20,24,25,28,48,55] The formate intensity maximum is at *ca.* 300–400 °C,[23,28] depending on the pretreatment and measurement conditions, with increasing intensities reported at lower temperatures.[48] All in all, formate coverage depends on the adsorption conditions (temperature, CO pressure) and

4.2. Formates: formation and decomposition

Formate species consist of a $HCOO^-$ unit connected to a surface zirconium cation *via* oxygen atom(s). Two different surface configurations have been proposed for the formate species: a bidentate formate[20,22,30,42] and a monodentate formate[22,42] shown in Fig. 11. The main IR bands of formate species on monoclinic zirconia are observed typically (see Fig. 12) at *ca.* 2965 cm^{-1}, 2880 cm^{-1}, 1565 cm^{-1}, 1387 cm^{-1}, 1379 cm^{-1} and *ca.* 1365 cm^{-1},[5,19,22,23,88] listed with their vibrations where they originated as well as theoretical

Fig. 11 Monodentate and bidentate formate species.

This journal is © The Royal Society of Chemistry 2015

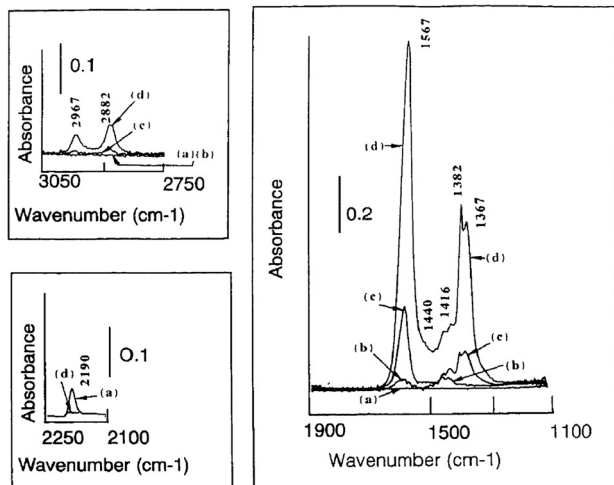*Catal. Sci. Technol.*, 2015, **5**, 3473–3490 | **3483**

Fig. 12 Formate and linear CO spectra at (a) 25 °C, (b) 150 °C, (c) 250 °C, and (d) 350 °C in 5% CO/He. Reprinted from ref. 20 with permission. Copyright 1993, Elsevier.

contact time with CO. With increasing temperature (240–400 °C), formate coverage decreases[23] while the formate intensity increases with increasing CO concentration in the gas phase.[23] Silver et al. have investigated adsorbed CO on pure ZrO_2 at 500 °C and they only discovered formates on the surface, and not (bi)carbonates or adsorbed CO species.[45]

At 250 °C, monodentate formate has a maximum at 1589 cm^{-1} and bidentate formate has maxima at 1568 cm^{-1}, 1388 cm^{-1} and 1371 cm^{-1}.[42] The authors also suggest that the formation of monodentate formate is intensified with increasing time of contact with CO, which is in agreement with the activated formation process, and that the shift from

bidentate to monodentate formates is due to repulsion among the bidentate formates at high surface concentrations[42] as shown with increasing time-on-stream (CO at 250 °C) at 1568 cm^{-1} separating into two bands at 1589 cm^{-1} and 1556 cm^{-1}.

According to Bianchi et al., the formate species would be probably bidentate as the difference between the observed bands at 1567 cm^{-1} ($\nu_{as}(OCO)$) and 1367 cm^{-1} ($\nu_s(OCO)$) is 200 cm^{-1},[20] and the same deduction has been used by Ma et al. for formate bands at 1570 cm^{-1} and 1361 cm^{-1},[7] both assigned to the species based on band separation. For carbonates, the typical difference should be ca. 100 cm^{-1} in the monodentate case and 300 cm^{-1} in the bidentate case.[89] Bianchi et al. also stated that another formate species might cause the band at 1382 cm^{-1}; however, it should also have a doublet band near 1570 cm^{-1}, close to that of the bidentate formate.[20]

Korhonen et al. have suggested a reaction scheme where bidentate formate formation proceeds via an activated monodentate complex.[22] They stated that based on DFT calculations, the formate is likely in a bidentate configuration as the monodentate one is unlikely to be stable.[22] Our investigations indicate a bridging bidentate formate configuration as the most stable geometry on all the tested surfaces.[28]

Formate forms on surface hydroxyl species. Pozdnyakov and Filimonov stated already in 1972 that formate is formed due to the reaction of CO with surface hydroxyls.[5] Yamaguchi et al. showed in 1978 the formation of formate and disappearance of terminal OH and multicoordinated OH bands following the adsorption of deuterated acetone-d_6, with terminal OH being more reactive toward formates than the multicoordinated one.[59] The amount of formate formed is

Table 6 Experimentally and theoretically[a] determined formate wavenumbers

Conditions (P_{CO}, T_{ads})	$\nu_{as}(COO) + \nu_s(COO)$ (cm^{-1})	$\nu(CH)$ (cm^{-1})	$\nu_s(COO) + \delta(CH)$ (cm^{-1})	$\nu_{as}(COO)$ (cm^{-1})	$\delta(CH)$ (cm^{-1})	$\nu_s(COO)$ (cm^{-1})	Ref.
Experimental							
1–60 Torr CO, 25 °C	2950–2850		—	1610–1580	1400–1350		5
100%, 25–500 °C	2950^b	2880	—	1580	1390	1360	19
100%, 400 °C	—^{c}	—^{c}	—	1575/1530	1386	1361	24
5% CO, 25–350 °C	2967	2882	2740	1567	1382	1367	20
162 kPa CO, 250 °C	2965	2881	—	1568–1550	1385	1370	42
4% CO, 25/250 °C	≈2970	≈2880	—	1570	1380	1365	30
100% CO, 350 °C	2973/2968	2889/2880	—	1570/1563	1390/1380	1361/1360	7
5%, 30–580 °C	2964	2881	2747	1564	1384	1365	22
8–65% CO, 240–400 °C	2969	2886	—	1560	1384	1371	23
5% CO, 100–550 °C	2960	3870	2755/2730	1568–1567	1386–1385	1367	28
Theoretical							
Bidentate to 2 Zr, (1̄11)	2915	2974	2754	1555	1394	1360	22
Bidentate to 1 Zr, (1̄11)	2845	2997	2676	1544	1375	1301	22
Bidentate to Zr and O, (1̄11)	2765	3138	2504	1585	1324	1180	22
Monodentate, (1̄11)	2843	2892	2473	1717	1347	1126	22
Bridging bidentate, (1̄11)	2914	2929	2773	1561	1420	1353	28
Bridging bidentate, (2̄12)	2901	2918	2721	1565	1385	1336	28
Bridging bid., (2̄12) corner	2860	2957	2694	1534	1368	1326	28

^{a} Combination modes ($\nu_{as}(COO) + \nu_s(COO)$ and $\nu_s(COO) + \delta(CH)$) for theory-based vibrations were obtained as a sum of the corresponding frequencies. ^{b} The band not originally assigned as a formate band rather as a methoxide band. ^{c} The author states that "the absorption in the 3000 cm^{-1} region is very weak" and a band near 2900 cm^{-1} is discernible in the spectrum.

3484 | Catal. Sci. Technol., 2015, 5, 3473–3490

This journal is © The Royal Society of Chemistry 2015

dependent on surface hydroxyls; a decrease in formate was shown by Jackson and Ekerdt through removal of water from a CO/H$_2$ feed[10] and by Bianchi et al. through dehydroxylation of the surface.[20] He and Ekerdt suggested that formate formation proceeds via gas-phase CO and a surface OH group.[21]

Formate formation has been reported at low temperatures (25 °C and 160 °C) on terminal OH (IR band at 3770 cm^{-1}).[20] In addition to formation on the terminal OH site, formate formation on multicoordinated OH (band at 3680 cm^{-1}) has been reported at higher temperatures (250–350 °C);[7,20,42] however, some experimental[23] and theoretical[22] results do not support the participation of the multicoordinated OH species. Jung and Bell suggested that the primary route for formate formation is via gas-phase CO and an OH group; after 9 hours at 250 °C and 162 kPa of CO, all terminal hydroxyl species as well as 38% of the bridged hydroxyl species are consumed in formate formation.[42] Based on their spectral evidence,[42] it seems that the consumption of terminal OH species is faster than that of multicoordinated OH species, yet whether all bridged hydroxyls can be consumed is unclear based on the evidence.

Jackson and Ekerdt suggested that formate formation in methanol synthesis involves an oxygen vacancy and an adjacent bridged hydroxyl site so that there is a terminal CO intermediate (the scheme is shown in Fig. 13).[10] However, their suggestion is in contradiction to some more recent results reporting that the terminal hydroxyls indeed participate in formate formation.[23,42]

Formate decomposition has been proposed to take place via two different pathways: dehydrogenation producing CO$_2$ and H$_2$ and dehydration releasing CO and H$_2$O, to follow the naming of He and Ekerdt.[21] Similar decomposition pathways have been proposed by Bianchi et al. suggesting the release

of CO and restoration of the OH groups,[20] and in our investigations suggesting that dehydration occurs in two separate reactions (first, reversible formate decomposition to CO restoring surface hydroxyls and then dehydroxylation to produce H$_2$O) as the dehydroxylation process is observed at a similar temperature range also without CO present in the gas phase.[28] A lower limit estimate for the activation energy of the dehydrogenation reaction is its reaction energy at 178–363 kJ mol^{-1} based on theory.[28] The typical temperature range for formate decomposition is above 300 °C,[28] and a desorption maximum has been reported at 410 °C.[20] The activated formate formation (increasing uptake rate up to 300 °C) and formate decomposition pathways are demonstrated in Fig. 14, where the zirconia sample is linearly heated from 100 °C to 550 °C in the presence of 2% CO and the y-axis corresponds to release/uptake from the sample.

Bianchi et al. have reported the amounts of CO, CO$_2$ and H$_2$ that have been adsorbed/desorbed during temperature-programmed desorption (TPD) after CO adsorption.[20] Not all carbon species are recovered, suggesting that the surface is not empty of formate (ca. 10% of CO adsorbed at 350 °C unaccounted for) by the end of the desorption process with T_{max} at 410 °C.[20] Based on the observed CO$_2$/H ratio, the surface species are claimed to be formate.[20] The formate decomposition routes have been reported to be either completely reversible decomposition resulting in restoration of the terminal hydroxyls[23] or partial (only about 20–40% of formate) decomposition forming hydrogen with reversible decomposition of the rest.[20,28] For ceria-based catalysts, the presence of co-adsorbed water in the catalyst significantly increased the rate of formate decomposition to CO$_2$ and H$_2$,[90,91] and the same likely applies to zirconia as well. Also, Korhonen et al. reported their observations of CO$_2$ as a product of formate decomposition above 500 °C.[22] The presence of an active
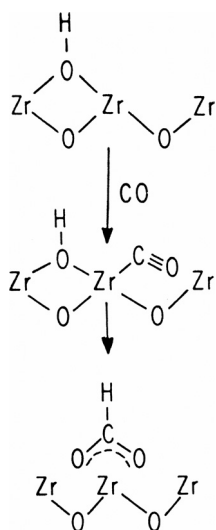
Fig. 13 Proposed formate formation mechanism as a part of methanol synthesis over ZrO$_2$. Adapted from ref. 10 with permission. Copyright 1986, Elsevier.

Fig. 14 Temperature-programmed surface reaction (TPSR) in the presence of CO on reduced ZrO$_2$. The y-axis corresponds to release (+) or uptake (−) from the sample. Reproduced from ref. 28 with permission from the PCCP Owner Societies.

This journal is © The Royal Society of Chemistry 2015

Catal. Sci. Technol., 2015, 5, 3473–3490 | 3485

View Article Online

Minireview

Catalysis Science & Technology

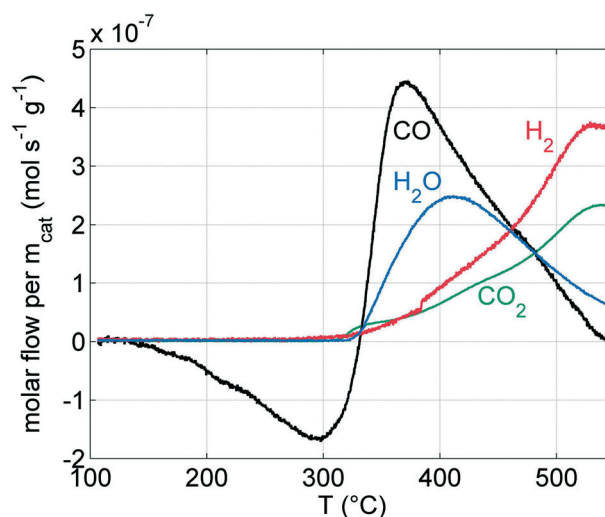metal (*e.g.* platinum) increases the rate of formate decomposition to CO_2 and H_2,[23] presumably by association of hydrogen (analogous to water-gas shift reaction), enabling a reasonable temperature window instead of 500 °C or higher.

The adsorption temperature has a significant effect on the amount of CO desorbed from the surface as CO_2 during TPD, yet the overall profile of the CO_2 desorption curve remains qualitatively similar.[30] CO desorption was clearly observable only after adsorption at 200 °C or 250 °C. At 250 °C, there are formates on the surface according to IR,[30] thus CO desorption is likely due to decomposition of surface formate species and CO_2 originates from formate or, especially after low-temperature adsorption of CO, (bi)carbonate species. The temperature of maximum desorption was in the range of 330 °C for CO_2 and 330–430 °C for CO desorbed after CO adsorption.

Köck *et al.* have investigated the adsorption of CO on ZrO_2 from room temperature up until 600 °C, yet their pretreatment (annealing at 900 °C and thereafter oxidation at 600 °C) of the sample has quenched most of the surface hydroxyls, leaving formate formation negligible and thus supporting the formate formation mechanism based on surface hydroxyl species.[62]

When CO adsorption at 85–250 °C is followed by cooling down to 25 °C, the intensity of the linear CO band at 2190 cm^{-1} is lower (by 12% with T_{ads} at 85 °C and 35% at 152 °C) with increasing pre-adsorption temperature compared to that for room temperature pre-adsorption.[20,55] This is assigned to

the formation of formate species at cationic Zr sites[54] which are thought to be the sites where CO adsorbs linearly.[6,18,27,29] When combined with our observations that formate formation at 100 °C in the presence of CO in the gas phase is accompanied by decreasing linear CO intensity (see Fig. 15),[28] it is suggested that site competition takes place and linear CO facilitates formate formation rather than gas-phase CO. Assuming a bidentate formate species formed on a terminal OH group and bound to a Zr cation (see Fig. 11), the cation site necessary for linear CO adsorption is blocked by the formate.

Measured amounts of adsorbed or desorbed CO reported in the literature are collected in Table 7. Increasing amounts of adsorbed/desorbed CO are reported with increasing adsorption temperature up to 350 °C.[20,30] Both Bianchi *et al.*[20] and Pokrovski *et al.*[30] have applied a similar TPD method, where adsorption is carried out at elevated temperature (T_{ads} in the table) followed by cooling to room temperature, and thereafter temperature-programmed heating begins. The amount of desorbed CO_x reported by Bianchi *et al.*[20] (0.12 µmol m^{-2}) is significantly lower than those reported by Pokrovski *et al.*[30] (0.35/1.34 µmol m^{-2}) after adsorption at 250 °C, while the specific surface areas are *ca.* 200 m^2 g^{-1} and 19/110 m^2 g^{-1}, respectively. The values reported in our recent work[28] seem to be larger than those by others; this might be due to a different experimental procedure, where weakly bound CO is not removed from the surface prior to temperature-programming.

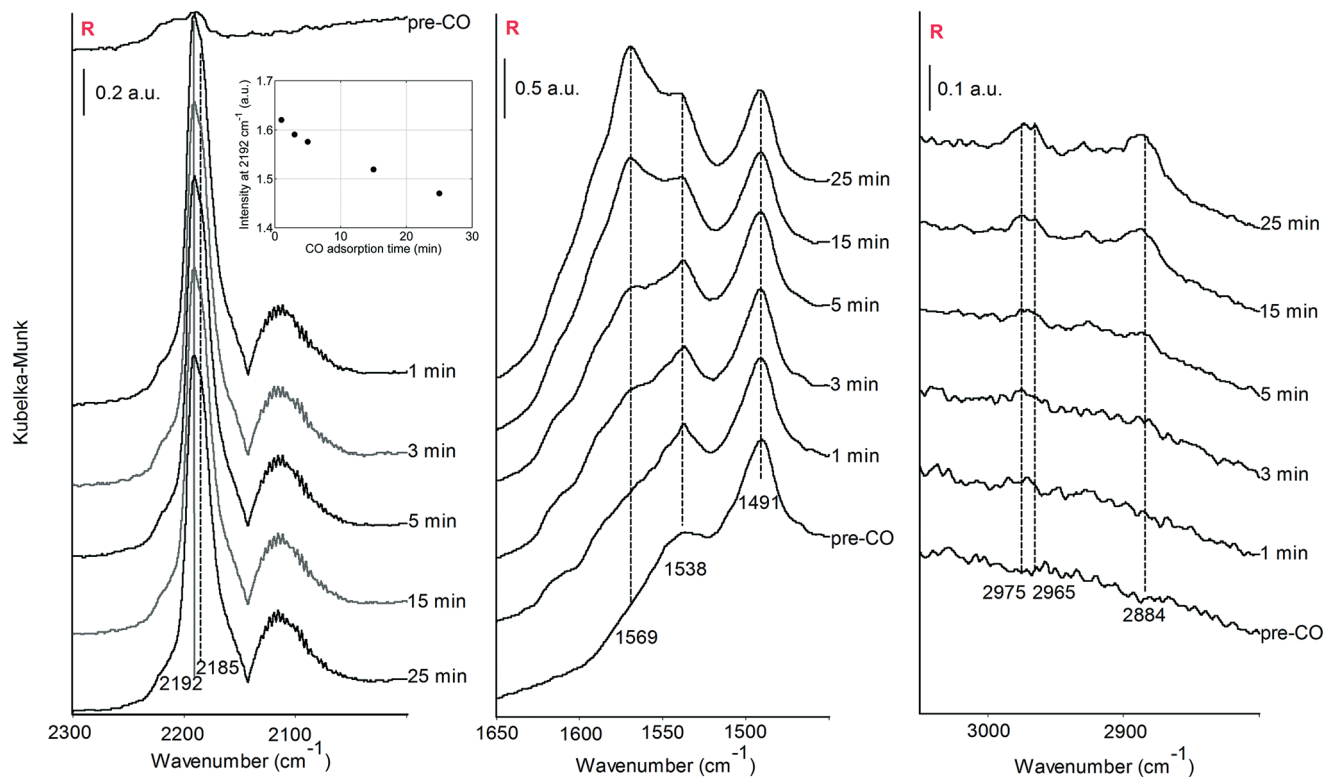**Fig. 15** Decreasing linearly adsorbed CO intensity (at 2192–2185 cm^{-1}) and increasing formate intensity (at 1569 cm^{-1}, 1538 cm^{-1}, 2975–2965 cm^{-1} and 2884 cm^{-1}) with time of contact with CO at 100 °C. Reproduced from ref. 28 with permission from the PCCP Owner Societies.

3486 | *Catal. Sci. Technol.*, 2015, **5**, 3473–3490

This journal is © The Royal Society of Chemistry 2015

Table 7 Adsorbed or desorbed CO amounts reported in the literature

Measurement	As reported	Scaled to μmol m^{-2}	T_{ads} (°C)	P_{CO}	t_{ads} (min)	Ref.
Adsorbed CO (MS)	0 μmol g^{-1}	0	25	5%	N/A	20
Adsorbed CO (MS)	10 μmol g^{-1}	0.050	150	5%	N/A	20
Adsorbed CO (MS)	26 μmol g^{-1}	0.13	250	5%	N/A	20
Adsorbed CO (MS)	37 μmol g^{-1}	0.19	350	5%	N/A	20
Desorbed CO$_x$ (MS)	6.5 μmol g^{-1}	0.033	150	5%	N/A	20
Desorbed CO$_x$ (MS)	23 μmol g^{-1}	0.12	250	5%	N/A	20
Desorbed CO$_x$ (MS)	33.6 μmol g^{-1}	0.17	350	5%	N/A	20
Desorbed CO$_x$ (MS)	0.09 μmol m^{-2} (SA = 19 m^2 g^{-1})	0.09	25	4%	20	30
Desorbed CO$_x$ (MS)	0.17 μmol m^{-2} (SA = 19 m^2 g^{-1})	0.17	150	4%	20	30
Desorbed CO$_x$ (MS)	0.22 μmol m^{-2} (SA = 19 m^2 g^{-1})	0.22	200	4%	20	30
Desorbed CO$_x$ (MS)	0.35 μmol m^{-2} (SA = 19 m^2 g^{-1})	0.35	250	4%	20	30
Desorbed CO$_x$ (MS)	0.51 μmol m^{-2} (SA = 110 m^2 g^{-1})	0.51	25	4%	20	30
Desorbed CO$_x$ (MS)	0.46 μmol m^{-2} (SA = 110 m^2 g^{-1})	0.46	150	4%	20	30
Desorbed CO$_x$ (MS)	0.59 μmol m^{-2} (SA = 110 m^2 g^{-1})	0.59	200	4%	20	30
Desorbed CO$_x$ (MS)	1.34 μmol m^{-2} (SA = 110 m^2 g^{-1})	1.34	250	4%	20	30
Adsorbed CO (gravimetric)	3–20 × 10^{17} mol m^{-2a}	0.5–3.3^a	500	1 atm	30	45
Net desorbed CO$_x$ at 100–550 °C (MS)	240–530 μmol g^{-1b}	2.7–5.9^b	100^b	2%	90^a	28

^{a} Depending on sample preparation temperature (600–900 °C). ^{b} Depending on pretreatment (hydration, reduction, reduction and hydration). CO contact first for 90 min at 100 °C, then continued during heating up to 550 °C.

As mentioned previously, the terminal OH group is the active species concerning formate or bicarbonate formation on the zirconia surface after gas-phase adsorption of CO at elevated temperature (240–400 °C).[23] The activity of the terminal OH group has been further investigated using isotope-labeled experiments with D$_2$O and D$_2$. When deuterated formates were formed *via* CO adsorption to OD (deuteroxyl) species, they could be transformed back to HCOO upon contact with hydrogen at 200 °C.[19] H/D isotope exchange of the surface formates with gas-phase D$_2$ seems to be possible, yet it is slow and competes with formate decomposition at around 300 °C.[26] Only 2–3% of the surface formate species are exchanged to DCOO species at 150 °C in 488 kPa of D$_2$.[42] The necessity of gas-phase D$_2$ for formate scrambling was demonstrated as the H/D exchange did not proceed between formates and surface deuteroxyls.[26] However, as formates can form on surface deuteroxyls by surface treatment with D$_2$O,[19] it is implied that once formed, formates are stable and do not scramble with each other *via* cleavage of the O$_{support}$–C bond.

4.3. Other species formed during interaction with CO

In addition to linear CO and formates, other species have also been observed during CO adsorption. These species reveal the diversity of interactions between CO and monoclinic zirconia although the number of reported observations remains low. The observed species include bidentate carbonates[48] and probably also carboxylate species as the band at 1416 cm^{-1} and its symmetric counterpart at 1560 cm^{-1} have been confirmed *via* difference spectra.[20] Monodentate carbonate (1469 cm^{-1}) and ionic carbonate bands (1303 cm^{-1} and 1442 cm^{-1}) were observed after CO adsorption at 350 °C.[7] Similarly, ionic carbonate and carboxylate species have been suggested to be present; their bands disappear when CO is

removed from the gas phase at 400 °C while the formate species remain intact.[54] When comparing CO adsorption at 350 °C on hydroxylated and dehydroxylated samples, the latter shows less intense formate bands but more intense bands at 1440 cm^{-1} and 1416 cm^{-1} as well as new bands at 1540 cm^{-1} and 1317 cm^{-1}, suggesting carbonates present on the surface and perhaps also carboxylate species.[20] Also, bidentate carbonates have been reported to form during high-temperature adsorption (above 250 °C) of CO.[48] Ma *et al.* have suggested that bicarbonate and carbonate species could be formed on ZrO$_2$ from CO *via* carboxylate surface species.[7] He and Ekerdt have suggested that CO is adsorbed on the metal oxide oxygen, forming a [COO] intermediate and then reacting further to form carbonate or formate.[21] All these species require the participation of one or two surface oxygen atoms.

CO adsorption followed by carbonate formation and CO$_2$ desorption leads to surface reduction as oxygen is removed from the surface. During temperature-programmed surface reaction (TPSR) in CO, CO$_2$ amounts detected correspond to 10–14% of surface oxygen atoms depending on the pretreatment of zirconia.[28] Pulse oxidation experiments show that with estimation of the monolayer coverage based on assuming a ZrO$_2$ (100) surface, 13.6% of the surface oxygen atoms can be removed by CH$_4$ at 900 °C.[92]

During static adsorption of CO at 200 °C and above, CO$_2$ formation was observed in the IR spectra, originating either from formate decomposition or from CO oxidation *via* lattice oxygen species.[62] Ionic carbonate was observed during CO adsorption at 150 °C and above on rehydrated zirconia, and it was released as CO$_2$ instead of CO.[20]

Silver *et al.* reported a small bicarbonate desorption peak during temperature-programmed heating in CO (25–620 °C), however, no gas-phase CO or IR bands of carbonates or bicarbonates were observed during CO exposure at 500 °C.[45] These

This journal is © The Royal Society of Chemistry 2015

Catal. Sci. Technol., 2015, **5**, 3473–3490 | 3487

observations suggest that formation of bicarbonates takes place below 500 °C, as expected based on the knowledge of bicarbonate species (for more information, see ref. 28 and references therein).

5. Future perspectives

As both monoclinic zirconia and its interaction with CO have been investigated for more than 40 years, in some regions, knowledge is still lacking. Surface configuration is one of the remaining questions, as the most stable surfaces according to density functional theory are different from those assumed based on HRTEM, yet the amount of independent experimental observations on clearly monoclinic samples remains few. The stability of the surface structure under the reaction conditions and during the reaction should be investigated carefully. Also, IR designation of terminal and multicoordinated hydroxyls (or any of the other interpretations) remains without irrefutable evidence, even though the multi-oxide studies by Tsyganenko and Filimonov[3,71] were very thorough in providing comparable information on several oxides with presumably different OH groups due to their crystal structure. Especially in the light of theoretical calculations suggesting mostly terminal and bibridged hydroxyl species, further confirmation of the assignment would provide more clarity. The Zr cations (Zr^{3+}, Zr^{4+}) have also caused some confusion; the basis for the IR assignment is unclear, yet the trivalent species have been successfully probed with N_2O.[6] The EPR assignment of Zr^{3+} species has also been under discussion.[8,46,47,51,57] Further information on surface vacancies and also surface defects, e.g., at the surface boundaries, could give a more thorough look at the surface interaction with hydroxyl and CO species. Also, tailoring the properties of monoclinic zirconia by using promoters and dopants without changing its crystalline phase could elucidate the interaction. Advanced methods similar to Raman in the case of ceria[93] might also provide surprisingly rich information.

The adsorbed CO species, especially the formate species, deserve more attention. The surface configuration of the species (monodentate, chelating or bridging bidentate) is unclear based on experimental observations, although bidentate species has been speculated and theoretical calculations suggest both chelating and bridging bidentate species. Also, the enthalpy of formation of formate species has only been estimated theoretically; an experimental confirmation for it, e.g., by microcalorimetry, would be welcome. Some clarity on the kinetics of formate formation on terminal and multicoordinated hydroxyls or even the extent of the reaction on both types of hydroxyls could provide new insights related to catalysis. Operando-style experiments with combined surface and gas-phase quantification would provide valuable input on all of the surface species with CO and hydroxyls. Observing the surface species with the same setup under vacuum might enlighten the mechanism of surface reduction

via oxygen removal and why evacuation is a more efficient reduction method than hydrogen treatment.[80]

To improve the modeling of carbon oxides, a better understanding of an active surface site is highly important to be able to set up more accurate computational surface models to better describe the complexity of the ZrO_2 support/catalyst. This would not only impact on the calculation of adsorption energies but also influence the calculated frequencies. As long as the nature of an active site is not known exactly, a systematic approach, where, e.g., different surface models are investigated side by side, is a natural choice to obtain information on adsorption characteristics. To discover the active surface sites and to further improve the selectivity of catalysts, nanoshaped supports and catalysts with surface regularity have proven to be interesting alternatives. The better the control over the surface sites, the better the catalyst selectivity. However, control is only to be reached through monocrystalline nanoshapes as the surfaces in polycrystalline shapes are not controlled.

Growing monoclinic zirconia in the shape of nanofibres and nanorods has gained some attention during the last 15 years, yet most of the shapes are polycrystalline. The preparation methods for monoclinic zirconia nanoshapes differ from traditional wet chemistry used for powder preparation. Nanorods have been prepared hydrothermally[16,17] in an autoclave, resulting in nanorods of various sizes, generally some tens of nanometers in diameter and a few hundred nanometers in length, with the length–diameter ratio ranging from ca. 5 up until 50 or even higher.

The exposed faces of the nanoshapes should be characterized with advanced electron microscopy techniques (e.g. aberration-corrected TEM as in ref. 94) to determine the orientation of the exposed surfaces. Boucher et al.[95] have tested different shapes of metal oxides with gold catalysts for steam reforming of methanol and water-gas shift, and concluded that the different shapes show somewhat different activities. Li and Shen[96] widely discussed the oxide shape effects in nanocatalysis, and mentioned some of the unknown issues with metal deposition on oxide nanoshapes, that is, whether the metal atoms are located on a single type of surface only. They also brought up the idea that the nanoshapes might not be stable under the reaction conditions, and this might also affect the metal–support interface, which is often considered to be the active site.[96]

6. Conclusions

A monoclinic zirconia surface has three kinds of coordinatively unsaturated cationic sites, two types of Zr^{4+} and one type of Zr^{3+}, coordinatively unsaturated Zr^{4+}–O^{2-} pairs, oxygen vacancies, terminal hydroxyls, and two types of multicoordinated hydroxyl species. The ratios of these sites can be modified with pretreatments by removing or adding oxygen and hydrogen from or to the surface through application of heat, vacuum or reactive atmospheres. The cationic sites are responsible for the linearly adsorbed CO species while formates are suggested to form preferably on sites where

unshielded zirconium ions are paired with terminal hydroxyl species, assuming a bidentate formate. This would provide an explanation for the submonolayer quantities of formate on zirconia. The concentrations of active sites for linear CO and formate formation are of similar magnitude, corresponding to *ca.* 5% of a monolayer or less, whereas the amount of hydroxyl species on the surface is roughly ten-fold higher. The formates as well as hydroxyl species prefer the defect types of Zr^{4+} sites. The specific roles of Zr^{3+} and terrace-type Zr^{4+} remain unclear. Other open questions include confirming the nature of the multicoordinated hydroxyls, the surface configuration of the formate species, and the energetics of formate formation. Nanoshapes might be a valuable tool in exploring the surface aspects related to formates and hydroxyls.

Acknowledgements

References

1 K. Tanabe and T. Yamaguchi, *Catal. Today*, 1994, **20**, 185–198.

2 T. Yamaguchi, *Catal. Today*, 1994, **20**, 199–218.

3 A. A. Tsyganenko and V. N. Filimonov, *J. Mol. Struct.*, 1973, **19**, 579–589.

4 A. Christensen and E. Carter, *Phys. Rev. B: Condens. Matter Mater. Phys.*, 1998, **58**, 8050–8064.

5 D. V. Pozdnyakov and V. N. Filimonov, *Zh. Fiz. Khim.*, 1972, **46**, 1011–1012.

6 T. M. Miller and V. H. Grassian, *Catal. Lett.*, 1997, **46**, 213–221.

7 Z.-Y. Ma, C. Yang, W. Wei, W.-H. Li and Y.-H. Sun, *J. Mol. Catal. A: Chem.*, 2005, **227**, 119–124.

8 C. Morterra, E. Giamello, L. Orio and M. Volante, *J. Phys. Chem.*, 1990, **94**, 3111–3116.

9 A. Trunschke, D. L. Hoang and H. Lieske, *J. Chem. Soc., Faraday Trans.*, 1995, **91**, 4441–4444.

10 N. B. Jackson and J. G. Ekerdt, *J. Catal.*, 1986, **101**, 90–102.

11 J. Li, J. Chen, W. Song, J. Liu and W. Shen, *Appl. Catal., A*, 2008, **334**, 321–329.

12 C. A. Franchini, A. M. Duarte de Farias, E. M. Albuquerque, R. dos Santos and M. A. Fraga, *Appl. Catal., B*, 2012, **117–118**, 302–309.

13 G. Águila, S. Guerrero and P. Araya, *Catal. Commun.*, 2008, **9**, 2550–2554.

14 K. Takanabe, K. Aika, K. Inazu, T. Baba, K. Seshan and L. Lefferts, *J. Catal.*, 2006, **243**, 263–269.

15 M. Benito, R. Padilla, L. Rodríguez, J. Sanz and L. Daza, *J. Power Sources*, 2007, **169**, 167–176.

16 X.-L. Liu, I. Pappas, M. Fitzgerald, Y.-J. Zhu, M. Eibling and L. Pan, *Mater. Lett.*, 2010, **64**, 1591–1594.

17 R. Espinoza-González, D. Diaz-Droguett, J. Avila, C. Gonzalez-Fuentes and V. Fuenzalida, *Mater. Lett.*, 2011, **65**, 2121–2123.

18 C. Morterra, R. Aschieri and M. Volante, *Mater. Chem. Phys.*, 1988, **20**, 539–557.

19 M.-Y. He and J. G. Ekerdt, *J. Catal.*, 1984, **87**, 381–388.

20 D. Bianchi, T. Chafik, M. Khalfallah and S. J. Teichner, *Appl. Catal., A*, 1993, **105**, 223–249.

21 M.-Y. He and J. G. Ekerdt, *J. Catal.*, 1984, **87**, 238–254.

22 S. T. Korhonen, M. Calatayud and A. O. I. Krause, *J. Phys. Chem. C*, 2008, **112**, 16096–16102.

23 P. O. Graf, D. J. M. de Vlieger, B. L. Mojet and L. Lefferts, *J. Catal.*, 2009, **262**, 181–187.

24 W. Hertl, *Langmuir*, 1989, **5**, 96–100.

25 K. T. Jung and A. T. Bell, *J. Mol. Catal. A: Chem.*, 2000, **163**, 27–42.

26 F. Ouyang, A. Nakayama, K. Tabada and E. Suzuki, *J. Phys. Chem. B*, 2000, **104**, 2012–2018.

27 V. Bolis, C. Morterra, M. Volante, L. Orio and B. Fubini, *Langmuir*, 1990, **6**, 695–701.

28 S. Kouva, J. Andersin, K. Honkala, J. Lehtonen, L. Lefferts and J. Kanervo, *Phys. Chem. Chem. Phys.*, 2014, **16**, 20650–20664.

29 E. Guglielminotti, *Langmuir*, 1990, **6**, 1455–1460.

30 K. Pokrovski, K. T. Jung and A. T. Bell, *Langmuir*, 2001, **17**, 4297–4303.

31 A. V. Radha, O. Bomati-Miguel, S. V. Ushakov, A. Navrotsky and P. Tartaj, *J. Am. Ceram. Soc.*, 2009, **92**, 133–140.

32 S. V. Ushakov and A. Navrotsky, *Appl. Phys. Lett.*, 2005, **87**, 164103.

33 H. F. Holmes, E. L. Fuller Jr. and R. A. Beh, *J. Colloid Interface Sci.*, 1974, **47**, 365–371.

34 J. Nawrocki, P. W. Carr, M. J. Annen and S. Froelicher, *Anal. Chim. Acta*, 1996, **327**, 261–266.

35 K. Dyrek, A. Adamski and Z. Sojka, *Ceram. Interfaces 2*, 2001, pp. 241–259.

36 K. Hadjiivanov, in *Advances in Catalysis*, ed. F. C. Jentoft, Academic Press, 2014, ch. 2, vol. 57, pp. 99–318.

37 J. Nawrocki, M. P. Rigney, A. McCormick and P. W. Carr, *J. Chromatogr. A*, 1993, **657**, 229–282.

38 C. Morterra, L. Orio and C. Emanuel, *J. Chem. Soc., Faraday Trans.*, 1990, **86**, 3003–3013.

39 C. Morterra, L. Orio, V. Bolis and P. Ugliengo, *Mater. Chem. Phys.*, 1991, **29**, 457–466.

40 G. Cerrato, S. Bordiga, S. Barbera and C. Morterra, *Appl. Surf. Sci.*, 1997, **115**, 53–65.

41 K. T. Jung, Y. G. Shul and A. T. Bell, *Korean J. Chem. Eng.*, 2001, **18**, 992–999.

42 K.-D. Jung and A. T. Bell, *J. Catal.*, 2000, **193**, 207–223.

43 I. A. Fisher, H. C. Woo and A. T. Bell, *Catal. Lett.*, 1997, **44**, 11–17.

44 N. E. Tret'yakov, D. V. Pozdnyakov, O. M. Oranskaya and V. N. Filimonov, *Russ. J. Phys. Chem.*, 1970, **44**, 596–600.

45 R. G. Silver, C. J. Hou and J. G. Ekerdt, *J. Catal.*, 1989, **118**, 400–416.

46 M. J. Torralvo, M. A. Alario and J. Soria, *J. Catal.*, 1984, **86**,

473–476.

47 M. Anpo and S. C. Moon, *Res. Chem. Intermed.*, 1999, **25**, 1–12.

48 J. Kondo, H. Abe, Y. Sakata, K.-i. Maruya, K. Domen and T. Onishi, *J. Chem. Soc., Faraday Trans. 1*, 1988, **84**, 511–519.

49 J. Kondo, Y. Sakata, K. Domen, K.-i. Maruya and T. Onishi, *J. Chem. Soc., Faraday Trans.*, 1990, **86**, 397–401.

50 M. Bensitel, O. Saur, J. C. Lavalley and G. Mabilon, *Mater. Chem. Phys.*, 1987, **17**, 249–258.

51 E. Giamello, M. Volante, B. Fubini, F. Geobaldo and C. Morterra, *Mater. Chem. Phys.*, 1991, **29**, 379–386.

52 V. Bolis, G. Cerrato, G. Magnacca and C. Morterra, *Thermochim. Acta*, 1998, **312**, 63–77.

53 D. Bianchi, J.-L. Gass, M. Khalfallah and S. J. Teichner, *Appl. Catal., A*, 1993, **101**, 297–315.

54 X. Mugniery, T. Chafik, M. Primet and D. Bianchi, *Catal. Today*, 1999, **52**, 15–22.

55 O. Dulaurent and D. Bianchi, *Appl. Catal., A*, 2001, **207**, 211–219.

56 J. Erkelens, H. T. Rijnten and S. H. Eggink- Du, *Recl. Trav. Chim. Pays-Bas*, 1972, **91**, 1426–1432.

57 M. G. Cattania, A. Gervasini, F. Morazzoni, R. Scotti and D. Strumolo, *J. Chem. Soc., Faraday Trans. 1*, 1989, **85**, 801–812.

58 K. Hadjiivanov and J.-C. Lavalley, *Catal. Commun.*, 2001, **2**, 129–133.

59 T. Yamaguchi, Y. Nakano and K. Tanabe, *Bull. Chem. Soc. Jpn.*, 1978, **51**, 2482–2487.

60 T. Yamaguchi, H. Sasaki and K. Tanabe, *Chem. Lett.*, 1973, **9**, 1017–1018.

61 P. A. Agron, E. L. Fuller Jr. and H. F. Holmes, *J. Colloid Interface Sci.*, 1975, **52**, 553–561.

62 E.-M. Köck, M. Kogler, T. Bielz, B. Klötzer and S. Penner, *J. Phys. Chem. C*, 2013, **117**, 17666–17673.

63 T. Merle-Méjean, P. Barberis, S. B. Othmane, F. Nardou and P. E. Quintard, *J. Eur. Ceram. Soc.*, 1998, **18**, 1579–1586.

64 P. D. L. Mercera, J. van Ommen, E. B. M. Doesburg, A. J. Burggraaf and J. R. H. Ross, *Appl. Catal.*, 1991, **71**, 363–391.

65 K.-H. Jacob, E. Knözinger and S. Benfer, *J. Mater. Chem.*, 1993, **3**, 651–657.

66 D. Martin and D. Duprez, *J. Phys. Chem.*, 1996, **100**, 9429–9438.

67 S. T. Korhonen, M. Calatayud and A. O. I. Krause, *J. Phys. Chem. C*, 2008, **112**, 6469–6476.

68 G. Mogilevsky, C. J. Karwacki, G. W. Peterson and G. W. Wagner, *Chem. Phys. Lett.*, 2011, **511**, 384–388.

69 A. Ignatchenko, D. G. Nealon, R. Dushane and K. Humphries, *J. Mol. Catal. A: Chem.*, 2006, **256**, 57–74.

70 A. N. Kharlanov, E. V. Lunina and V. V. Lunin, *Russ. J. Phys. Chem.*, 1997, **71**, 1504–1509.

71 A. A. Tsyganenko and V. N. Filimonov, *Spectrosc. Lett.*, 1972, **5**, 477–487.

72 K. Yardley, *Mineral. Mag.*, 1926, **21**, 169–175.

73 D. K. Smith and W. Newkirk, *Acta Crystallogr.*, 1965, **18**, 983–991.

74 O. Syzgantseva, M. Calatayud and C. Minot, *J. Phys. Chem. C*, 2010, **114**, 11918–11923.

75 J. D. McCullough and K. N. Trueblood, *Acta Crystallogr.*, 1959, **12**, 507–511.

76 C. Warble, *Ultramicroscopy*, 1984, **15**, 301–309.

77 W. Piskorz, J. Gryboś, F. Zasada, S. Cristol, J.-F. Paul, A. Adamski and Z. Sojka, *J. Phys. Chem. C*, 2011, **115**, 24274–24286.

78 K. Momma and F. Izumi, *J. Appl. Crystallogr.*, 2011, **44**, 1272–1276.

79 M. C. Deibert and R. Kahraman, *Appl. Surf. Sci.*, 1989, **37**, 327–336.

80 K.-O. Axelsson, K.-E. Keck and B. Kasemo, *Appl. Surf. Sci.*, 1986, **25**, 217–230.

81 K.-H. Jacob, E. Knözinger and S. Benfer, *J. Chem. Soc., Faraday Trans.*, 1994, **90**, 2969–2975.

82 O. A. Syzgantseva, M. Calatayud and C. Minot, *J. Phys. Chem. C*, 2012, **116**, 6636–6644.

83 M. Van Thiel, E. D. Becker and G. C. Pimentel, *J. Chem. Phys.*, 1957, **27**, 486–490.

84 M. L. Cerón, B. Herrera, P. Araya, F. Gracia and A. Toro-Labbé, *J. Mol. Model.*, 2013, **19**, 2885–2891.

85 I. M. Iskandarova, A. A. Knizhnik, E. A. Rykova, A. A. Bagatur'yants, B. V. Potapkin and A. A. Korkin, *Microelectron. Eng.*, 2003, **69**, 587–593.

86 G. N. Vayssilov, M. Mihaylov, P. S. Petkov, K. I. Hadjiivanov and K. M. Neyman, *J. Phys. Chem. C*, 2011, **115**, 23435–23454.

87 F. Ouyang, J. N. Kondo, K.-C. Maruya and Domen K., *J. Chem. Soc., Faraday Trans.*, 1996, **92**, 4491–4495.

88 G. Busca, J. Lamotte, J. C. Lavalley and V. Lorenzelli, *J. Am. Chem. Soc.*, 1987, **109**, 5197–5202.

89 G. Busca and V. Lorenzelli, *Mater. Chem.*, 1982, **7**, 89–126.

90 T. Shido and Y. Iwasawa, *J. Catal.*, 1992, **136**, 493–503.

91 T. Shido and Y. Iwasawa, *J. Catal.*, 1993, **141**, 71–81.

92 J. Zhu, J. van Ommen, H. Bouwmeester and L. Lefferts, *J. Catal.*, 2005, **233**, 434–441.

93 S. Agarwal, X. Zhu, E. J. M. Hensen, L. Lefferts and B. L. Mojet, *J. Phys. Chem. C*, 2014, **118**, 4131–4142.

94 S. Agarwal, L. Lefferts, B. L. Mojet, D. A. J. M. Ligthart, E. J. M. Hensen, D. R. G. Mitchell, W. J. Erasmus, B. G. Anderson, E. J. Olivier, J. H. Neethling and A. K. Datye, *ChemSusChem*, 2013, **6**, 1898–1906.

95 M. B. Boucher, S. Goergen, N. Yi and M. Flytzani-Stephanopoulos, *Phys. Chem. Chem. Phys.*, 2011, **13**, 2517–2527.

96 Y. Li and W. Shen, *Chem. Soc. Rev.*, 2014, **43**, 1543–1574.

3490 | *Catal. Sci. Technol.*, 2015, **5**, 3473–3490

This journal is © The Royal Society of Chemistry 2015